Nucl. Fusion **53** (2013) 027003 (23pp) doi:10.1088/0029-5515/53/2/027003

CONFERENCE REPORT

Summary of the ARIES Town Meeting: 'Edge Plasma Physics and Plasma Material Interactions in the Fusion Power Plant Regime'

M.S. Tillack[1], A.D. Turnbull[2], C.E. Kessel[3], N. Asakura[4], A.M. Garofalo[2], C. Holland[1], F. Koch[5], Ch. Linsmeier[5], S. Lisgo[6], R. Maingi[7], R. Majeski[3], J. Menard[3], F. Najmabadi[1], R. Nygren[8], T.D. Rognlien[9], D.D. Ryutov[9], R.D. Stambaugh[2], P.C. Stangeby[10] and D.P. Stotler[3]

[1] UC San Diego, La Jolla, CA 92093-0417, USA
[2] General Atomics Inc., La Jolla, CA, USA
[3] Princeton Plasma Physics Laboratory, Princeton, NJ, USA
[4] Japan Atomic Energy Agency, Naka, Ibaraki 311-0193, Japan
[5] Max-Planck-Institut für Plasmaphysik, EURATOM Association, 85748 Garching b. München, Germany
[6] ITER Organisation, F-13067 Saint Paul-lez-Durance Cedex, France
[7] Oak Ridge National Laboratory, Oak Ridge, TN, USA
[8] Sandia National Laboratories, Albuquerque, NM, USA
[9] Lawrence Livermore National Laboratory, Livermore, CA, USA
[10] Institute for Aerospace Studies, University of Toronto, 4925 Dufferin Street, Toronto, M3H 5T6, Canada

Received 31 July 2012, accepted for publication 31 December 2012
Published 25 January 2013
Online at stacks.iop.org/NF/53/027003

Abstract
This review summarizes the presentations and discussions by experts in the fields of edge plasma physics and plasma–material interactions at a workshop organized for the purpose of evaluating current status and extrapolating forward to the post-ITER power plant regime. The topics included physics, modelling, experimental results, benchmarking and programme planning.

(Some figures may appear in colour only in the online journal)

1. Introduction

The plasma–material interface has long been recognized as a major challenge in the utilization of high-temperature plasmas for fusion energy applications. The combination of the generation of energetic alpha particles and the use of any auxiliary heating in a fusion device results in substantial plasma energy that is exhausted from the device on an energy confinement time. The resulting peak heat fluxes on plasma-facing components (PFCs) can be very large owing to the use of magnetic divertors that concentrate the exhaust in specific locations, though substantial heat fluxes can also flow to other wall components. Despite its importance, our understanding of the edge plasma and its interactions with surrounding structures remains insufficient to predict either steady or transient heat and particle loads on components, which is a prerequisite in order to transition from experimental research to energy applications.

The majority of the world's resources devoted to this subject have been concentrated on existing experiments and ITER. It is becoming increasingly urgent to expand our predictive capabilities to future nuclear facilities and power plants. To that end, the ARIES Team hosted a 'Town Meeting' on Edge Plasma Physics and Plasma Material Interactions in the Fusion Power Plant Regime. ARIES Town Meetings are held occasionally in response to programmatic needs that align with the current mission of the ARIES Team. These meetings provide an opportunity for increased interactions

between researchers in the field and the power plant design community.

The aim of this workshop was to bring together several communities that do not normally interact, namely plasma theorists, modellers and experimentalists together with reactor designers, materials scientists and engineers. A major goal was to initiate modelling efforts for a reactor scenario beyond the current focus of ITER modelling, since it is now reasonably clear that the solutions needed for the plasma–material interface in DEMO will be significantly different from ITER (see section 2.2). The workshop was also intended as a follow-on from the successful International High Heat Flux Component Workshop on Readiness to Proceed from Near Term Fusion Systems to Power Plants, held in December 2008, where many of these issues were identified and fleshed out [1].

In addition, the workshop was intended to serve as a snapshot of the status of these efforts as of May 2010. The reports presented in this paper are not intended to be comprehensive, and are focused on those issues that were specifically addressed at the workshop. The key questions addressed in this Town Meeting included the following:

(1) What is the status of our current understanding and predictive capabilities in edge plasmas and plasma–material interaction (PMI)?
(2) What R&D are needed in order to advance this field towards the power plant regime?
(3) What contributions can new devices make towards advancing this field?

The workshop participants comprised 42 researchers from 17 organizations, including the US, EU and Japan, who participated in the two-day meeting held in the campus of the University of California in San Diego. The agenda comprised seven sessions:

(1) Background and power plant requirements.
(2) Physics of the edge: current understanding and projections to ITER and power plants.
(3) Modelling of the tokamak edge.
(4) Experimental benchmarking of models for power plants.
(5) Innovative solutions.
(6) New device contributions to edge physics benchmarking.
(7) Conclusions and future plans.

Two of the sessions—'Experimental benchmarking of models for power plants' and 'New device contributions to edge physics benchmarking'—were organized as directed panel discussions. These panels were both lively and productive. More details on the meeting can be found at the meeting website[11].

Several important issues were identified at the workshop and are discussed in this report. Section 2 sets the background: while considerable progress is being made in addressing the interaction of the edge plasma with PFCs in ITER (section 2.1), not all of the proposed solutions will be applicable in a DEMO reactor (section 2.2). The key difference is the total fluences expected in DEMO rather than the energy, radiation and particle fluxes alone. In addition to the much larger fluences, the complication from the presence of hot walls is an additional important consideration requiring further research. The specific requirements for handling heat fluxes are discussed in section 2.3.

Section 3 focuses on physics issues. In section 3.1, similarity experiments are described, scanning the dimensionless physics parameters ρ^*, ν^* and β, which have recently been performed in DIII-D, NCSX and C-Mod to determine the divertor heat-flux scaling. Edge-localized mode (ELM)-free operation is a promising route that avoids the serious issue of transient heating in the divertor, and several new regimes appear to be promising (section 3.2), but in all cases, the key unknown is the scaling to reactor configurations.

Some modelling efforts for a DEMO reactor configuration are in progress, initiated partly as a response to the call for papers to this workshop. In modelling of the DEMO-level Slim-CS divertor with the SONIC code (section 4.1), it was found that appropriate choices for the PFC, structure material (SM) and cooling system are more restricted than in ITER due to the significant neutron irradiation and high operation temperature. In section 4.2, extensive modelling is presented using the UEDGE models of edge plasma characteristics and wall fluxes for a number of existing tokamaks as well as ITER and some ARIES designs. In addition, a number of enhancements have been added to improve future modelling: coupling UEDGE with the BOUT three-dimensional (3D) turbulence code, and the addition of kinetic effects applicable to a hot wall as envisaged in a DEMO. In section 4.3, the problems involved in neutral transport modelling and recycling between the PFC materials and plasma in a reactor environment are described. The major new element in a DEMO is the interaction with a hot wall. Models are being developed but will need validation.

In terms of benchmarking, which was the focus of the first of the two directed panel discussions (section 5), the major concern that became apparent was that it is not clear how benchmarking codes can be achieved for conditions in an actual reactor environment given the absence of any experimental facilities approaching these parameters. While ITER will provide a significant step with a burning plasma, albeit at a low fluence, it is not at all clear whether this will be sufficient to adequately test the models. This issue is serious and will require much more additional work.

In the session on innovative concepts, the 'snowflake' (section 6.1) and Super-X divertors were presented as promising techniques for reducing localized heat fluxes to divertor plates. However, in scaling the snowflake divertor to a DEMO reactor, a key issue is whether the poloidal field coils required can be placed outside the shield and possibly outside the toroidal field (TF) coils, as well as the additional volume required for these concepts. This is not entirely clear, but the prospect is improved by the possibility of a more compact reactor design. Liquid metal PFCs are an option for separating the plasma-facing material from the structures. Liquid metals can withstand the neutron environment and present many advantages as a PFC. The supporting substrate can then be optimized separately for its structural function in the neutron environment. The issue becomes one of compatibility of the liquid metal with the plasma–vacuum interface and the structure interface, but a number of options are available that are discussed in section 6.2. Carbon still presents possibilities as a suitable PFC despite its reputation as unsuitable because

[11] http://cer.ucsd.edu/ATMPMI2010.

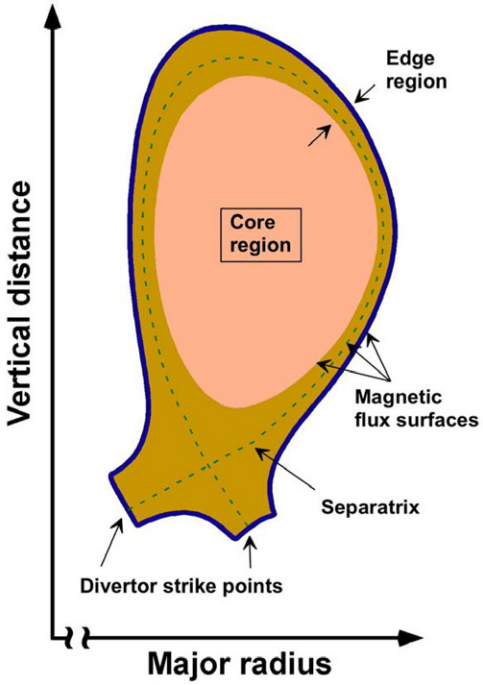

Figure 1. Poloidal cross-section of a single-null tokamak plasma.

of its T retention properties. Recent research (section 6.3) has shown that at higher wall temperatures, the T retention is small. In addition, since material from the walls is continually deposited on the divertor, erosion of the divertor may not be an issue.

The possible contributions of new devices to modelling efforts were discussed in a final panel session (section 7). Four facilities currently being proposed were discussed: two Fusion Nuclear Science Facilities (FNSFs) at different aspect ratios, and two non-nuclear tokamak PMI facilities. The general consensus was that all would provide useful data; either a FNSF or a dedicated PMI facility would reduce the risk of the large step between ITER and a DEMO at some additional cost. A non-nuclear PMI facility would probably result in lower cost but greater risk in extrapolation to a reactor.

Figure 1 shows a poloidal cross-section of a single-null plasma similar to that of ITER. The figure depicts the main features of the plasma edge region, including the separatrix (that separates the closed and open field lines) and the strike points where the separatrix meets the divertor surfaces.

2. Background and power plant requirements

2.1. Description of ITER's edge regime

For high-power density, reactor-scale magnetic confinement devices such as ITER [2–4], the plasma edge regime must be consistent with the core plasma purity and power exhaust requirements, while at the same time preserving the integrity of the PFCs that make up the wall of the containment vessel. Successful operation requires that this constraint be met for all phases of the discharge: start-up, the plasma current 'flat-top' (quasi-steady conditions that are maintained for most of the discharge) and controlled termination, each of which is associated with different edge plasma regimes. A stipulated number of transient events (large type-I ELMs, monster sawteeth and disruptions) must also be accommodated without significant damage to PFCs, but this relates more to the active mitigation systems (ELM and sawtooth control, rapid shutdown) than to the inherent properties of the edge plasma, and so is not discussed further here. A principal objective for ITER is the generation of a deuterium and tritium (D–T) fuelled discharge with a 400 s flat-top during which the power generated is ten times larger than the amount used to heat the plasma ($Q = 10$) [5].

Plasma purity is important during start-up since contamination increases the plasma resistance and inductance, causing a larger fraction of the available voltage swing from the solenoid to be consumed when ramping the plasma current, and thereby decreasing the length of the flat-top. The plasma is in direct contact with the main wall during the initial phase of start-up, and so the influx of impurities to the core can be relatively large. For this reason, and to avoid exceeding the engineering heat-flux limit on the main wall panels ($5\,\mathrm{MW\,m^{-2}}$) [6] when auxiliary heating is applied, an X-point is formed as quickly as possible after breakdown ($\sim$10 s). This diverts the plasma boundary away from the main wall and onto target plates, which have a higher maximum heat-flux rating ($10\,\mathrm{MW\,m^{-2}}$) and are remote from the core. However, the transport of impurities from the targets to the core can still be larger during this early phase of start-up than for the flat-top since the former has an edge plasma with comparatively low density and high temperature. For targets made of carbon, as in the initial ITER configuration, this is of moderate concern since carbon has a low atomic number and can therefore be tolerated at high core concentrations ($\sim$1%). The situation is different after tungsten targets are installed for D–T operation, as currently planned, since relatively small amounts of tungsten reaching the core will compromise the discharge. Studies in existing machines are underway that will help in improving the models used for optimizing the ITER start-up sequence.

For the flat-top phase, meeting the $Q = 10$, 400 s milestone requires that ITER operates in the enhanced confinement mode, or H-mode. There are several types of H-mode and most involve intense, periodic bursts of plasma into the boundary, known as ELMs. They result in increased particle and energy fluxes to the targets for a duration of several hundred microseconds, and if energetic enough, may produce filamentary plasma structures that extend far into the edge that can interact with the walls of the main chamber outside the divertor region. Type-I ELMs are the most common and powerful [7], and type-I ELMy H-mode data are the basis of the empirical scaling used to predict ITER's energy confinement. However, laboratory studies of prototype target plate PFCs for ITER have shown that they cannot withstand the level of thermal cycling associated with type-I ELMs in a $Q = 10$ discharge, and so an alternative plasma scenario must be employed. The current options are ELM size control via pellet pacing [8] or resonant magnetic perturbations (RMPs) [9], small ELM regimes at reduced energy confinement [10, 11] or sustained ELM-free H-mode plasmas, which are challenging due to the narrow range of operational space over which they are observed to occur [12–15] (see also section 3.2).

Because the ELMs are brief, the majority of the core particle and power exhaust during H-mode takes place during inter-ELM periods. This relatively quiescent plasma, which can also include regimes that have very small, rapid ELMs or are ELM-free, is referred to here as the 'quasi-steady' edge conditions. This sounds contradictory for ELMy H-modes, but is reasonable in the sense that the inter-ELM periods are usually far longer than the relevant transport timescales (∼1 ms). For the quasi-steady conditions, it is necessary to operate with a 'detached' edge plasma [16], where a large temperature gradient parallel to the magnetic field lines is formed between the core and the targets. The temperature drop is controlled by deuterium or impurity gas injection, or both. An important property predicted for the ITER plasma boundary is that it will be thick and hot enough that neutral deuterium particles will not reach the core, which is rarely the case in present-day tokamaks, where fuelling is usually accomplished via gas puffing into the plasma edge (ITER will rely on cryogenic pellets). If true, this will give some flexibility to adjust the edge plasma density independently of the confined plasma, making detachment control more straightforward. Impurity radiation in the edge will need to dissipate approximately 75% of the power exhausted from the core in order to reduce the heat flux at the targets to acceptable levels. Good detachment control is important at such high radiated power fractions since there is the potential for runaway edge plasma cooling, where the emission zone can penetrate the core and trigger a radiative collapse and possibly a disruption. The plasma near the targets becomes 'detached' when the local temperature drops below a few eV, at which point neutral particles from plasma recycling have large mean free paths and plasma momentum can be lost to the wall via neutral–plasma collisions [17], thereby reducing the plasma flux to the target. Detachment is critical because when incident hydrogen ions recombine with electrons on a material surface, ∼10 eV of potential energy per particle is deposited as heat. This process is enough to keep the heat flux above 10 MW m^{-2} in ITER if the particle flux is not reduced via momentum loss, even for very cold plasmas [18].

As mentioned above, one possible method for ELM control is the application of so-called RMPs, as observed on the DIII-D tokamak [9]. The fields on ITER will be generated by a complex system of coils that are located inside the vacuum vessel but behind the neutron shield. The RMPs should reduce the ELM size, but they will break the toroidal symmetry of the magnetic field geometry in the edge, which can generate localized high-heat-flux regions on the targets [19]. To moderate this effect, the ITER RMP coil system is being designed to enable rotation of the perturbation in the toroidal direction with a frequency of 0.1–1 Hz in order to spread out the incident power.

Controlled termination of the plasma at the end of the flat-top is difficult because the particle inventory and stored energy must be dissipated while avoiding contact with the main wall. The issues arise from a natural tendency for the position of ITER-shaped plasmas to become vertically unstable if certain discharge parameters are not maintained, or rapidly shift horizontally after the transition out of H-mode, which occurs when the power exhausted from the core drops below a critical level. The challenge comes from two significant differences between ITER and present-day tokamaks: low pumping rate, to minimize the required tritium throughput, and long magnetic control response time, which results from the superconducting coils and the thick, conductive vacuum vessel for neutron shielding and management of disruption forces. Both of these features are expected to be design requirements for any future reactor-scale device as well.

2.2. Edge plasma and PMI concerns for fusion power plants

The requirements on the design of high-power density, reactor-scale magnetic confinement devices are interdependent. For example, the PFC requirements cannot be isolated from the core plasma performance parameters (density, confinement time, bootstrap current fraction, etc), nor can they be isolated from the requirements on the overall design of the plant built to produce and recover power, and utilize a tritium-breeding blanket. Nevertheless, while the requirements for detailed design integration with the blanket or for remote maintenance are important, the focus here is on the interdependent requirements between the core plasma and PFC materials.

Integrated solutions are needed to ensure that the plasma edge is consistent with the core plasma, power and particle exhaust requirements, and interactions with PFCs. A number of significant differences between ITER and a power reactor will require different solutions to issues at the interface between the plasma and surface materials. Most notably, power plants will operate in a significantly more severe nuclear environment. The pulse length will be much longer (a year compared with 500–3000 s) and the effective duty cycle should approach 100%, resulting in a large increase in the total neutron and plasma particle fluences. This has implications for the choices of materials, maintenance, and also in options for diagnostics and plasma control. In addition, as a result of the longer pulse length, longer timescale PMI processes will be important, primarily erosion and migration, dust accumulation and tritium retention. Another major consideration is the requirement of hot walls in a power plant to achieve high thermal conversion efficiency, which significantly changes the chemistry and material evolution at the plasma–vacuum interface.

Table 1 is a summary of the expected discharge characteristics relevant to PFC interactions for ITER and an example power reactor. The values shown for a power plant are based on the recent ARIES-ACT1 design [20]. The spectrum of concepts for tokamak (and non-tokamak) power plants includes designs with more conservative assumptions.

With the construction of ITER, we are gaining insight into the complexity of the design integration necessary in a long-pulse DT device and in resolving multiple overlapping and conflicting requirements, including how power from the plasma will be distributed onto the divertor, first wall and other in-vessel components, and how large transient heat loads from disruptions and ELMs will be mitigated. As is already apparent in ITER, a tremendous amount of information about design detail and integration must be developed to understand whether a design actually performs under plasma and nuclear loading conditions. There is nothing yet approaching this level of detail for fusion DEMO and power plants. A comprehensive solution will require self-consistent edge plasma conditions,

Table 1. Comparison of expected discharge characteristics relevant to PFC interactions between ITER and an advanced tokamak power plant.

	ITER (DT inductive)	Power plant[a]
Fusion power (MW)	500	1800
Pulse length (s)	300–500	Steady state ($>10^6$)
Alpha heating power (MW)	100[b]	360
Additional heating input (MW)	73[b]	45
Radiated power to first wall (MW)	25–40	115
Average neutron wall load (MW m^{-2})	$\geqslant$0.5	2.45
Peak neutron wall loading (MW m^{-2})	0.76	3.6
Peak neutron fluence over plant lifetime (MW yr m^{-2})	0.3	144[c]
Effective duty cycle[d]	5%	80%
Peak wall temperature (°C)	400	1000
Total plasma volume (m^3)	830	582
Pedestal pressure (MPa)	0.11	0.128
Total plasma stored energy (MJ)	375[e]	691
Total power (including nuclear) to the divertor (MW)	204	455
Maximum design heat flux in divertor (MW m^{-2})[b,f]	10	15
Pedestal energy (MJ)[g]	136	117
Type-I ELMs unmitigated thermal release (MJ)[h]	27	24
ELM energy density to inboard divertor (MJ m^{-2})[i]	13.5	0
ELM energy density to outboard divertor (MJ m^{-2})[i]	5.33	11.3
Type-I ELMs mitigated thermal release (MJ)[b,j]	0.60	
He flux to the divertor (m^{-2} s^{-1})[k]	10^{22}	3.5×10^{22}
D_2 flux to the divertor (m^{-2} s^{-1})[k]	10^{24}	3.5×10^{24}
He flux to the first wall (m^{-2} s^{-1})[k]	10^{17}	3.5×10^{17}
D_2 flux to the first wall (m^{-2} s^{-1})[k]	10^{21}	3.5×10^{21}

[a] Parameters taken from ARIES-ACT1 [20] except where indicated.
[b] Heat and Nuclear Loading Specifications from ITER_2LULDH_v2_3.doc (November 2009), without errors.
[c] Power plant assumes 40 full power years.
[d] For ITER this is taken as the product of the discharge duty cycle (25%) and fractional operation time in a year. For a power plant, it is the projected availability of 0.8.
[e] From [6].
[f] Partially or fully detached divertor operation, and set at the maximum tolerable value.
[g] From $W_{ped} = 3/2$ times integrated $p_{ped} \times dV_{plasma}$.
[h] Assumed to be 20% W_{ped}.
[i] Single-null energy split of 2/3 to IB and 1/3 to OB; double-null energy split of 100% to OB and 65% to each divertor.
[j] Determined to avoid melting and cracking in ITER.
[k] ITER values taken from A.S. Kukushkin, 14.04.08 ITER_D_27TKC6. For the power plant case, it is assumed that particle fluxes scale with fusion power and inversely with the major radius.

presumably through a H-mode pedestal, He removal, wall conditions capable of handling the radiation, energy and particle fluxes, and with adequate T retention properties, and a full divertor system capable of handling the necessary heat fluxes.

The heat fluxes to divertors and the wall, including neutron and radiation fluxes, are a focus of great concern in ITER and much work has been done in this area. Some progress has also been made on identifying the new issues that arise in a power plant and these are discussed in the following section. However, a large gap remains in existing knowledge of the dispersal of particle flux to the wall and the subsequent wall–particle interactions. Although ITER will operate with higher temperature walls than existing tokamaks and can provide some data to fill this gap, a power reactor is expected to operate with walls at still higher temperatures. This changes some of the basic particle–wall interactions and this will need to be addressed. ITER cannot answer all of the questions needed to proceed to a full reactor design.

As in ITER, a power reactor is envisaged to operate with a H-mode edge in order to achieve sufficient confinement. In tokamaks, the edge pedestal will strongly impact the interior profiles, and therefore several key performance parameters. Larger and steeper pedestals yield higher performance (e.g. better confinement) in the core but also result in periodic ELMs that release large energy pulses in very short timescales ($\sim$ a few hundred microseconds). For ITER, the expected ELM strength and frequency are an issue for the integrity of the PFCs and solutions are being developed (section 2.1). Development of a self-consistent solution for power plants capable of handling the expected fluxes is even more crucial, due to the higher required availability and more severe regulatory requirements on commercial systems. This means either reducing or eliminating the ELM size or developing more innovative solutions to handle them. The option of reducing or eliminating ELMs is difficult given the strong dependence of both the core parameters and the ELM size on maintaining a steep pedestal, but some potential solutions are described in section 3.3.

The alternative option of developing unconventional solutions is discussed in section 6. One strategy for resolving some of the issues is to separate the PFCs from the substrate.

Then the materials facing the plasma can be optimized for the heat, particle and radiation fluxes, and the substrate for resilience, strength, lifetime, etc. Flowing liquid walls and self-passivating tungsten walls are two such ideas.

2.3. Requirements for high-heat-flux components

The high-heat-flux components for a DEMO or power plant cannot be isolated from the overall design of a plant built to produce and harvest power and utilize a tritium-breeding blanket. To produce energy efficiently, we must use the (∼20%) power going to the divertor; so the divertor must be integrated with heat removal from the blanket. Typically a solid first wall is an integral part of the blanket. Highly efficient energy conversion (e.g. with a Brayton cycle) and He cooling require a refractory structure for the divertor, or another approach, such as a liquid surface, and compatible integration with the first wall and blanket.

The high-heat-flux components include the first wall integrated with the blanket, the divertor and specialized in-vessel components that face the plasma, such as launching structures for RF systems. The basic issues of concern for these components are heat removal, transient heat and electromagnetic loads, neutron damage, erosion and tritium retention. The functional requirements of these components are that they perform within set operational limits for loads and temperatures and have adequate lifetime. To fulfil such requirements we set specifications (e.g. maximum temperature or creep strength or component deformation) after examining the limits that technology can provide. We have typically done this in design studies using materials properties and some experience from high-heat-flux tests as the basis for estimating performance.

For fidelity in such designs, we should have the following:

(1) heat and particle fluxes consistent with the current state of knowledge, for example, what has been learned in the last few years in the ITER project about the distribution of heat and particle loads for steady-state operation and transient events;
(2) choices of materials that are consistent with the current state of knowledge and recognition of issues with regard to their ranges of service temperatures and responses to threats from the fusion environment, such as degradation of mechanical or thermal properties due to damage from energetic particles (including neutrons) and related effects on tritium retention and production of dust;
(3) sound engineering practices; and
(4) credible integration of systems.

Another different type of requirement, discussed in the last portion of this section, is a credible path for development of such components.

For divertors with high-heat loads (5–10 $\mathrm{MW\,m^{-2}}$), ferritic steels do not have the required thermal conductivity (∼100 $\mathrm{W\,m^{-1}\,K^{-1}}$) combined with adequate strength at the desired maximum allowable temperature (>1000 °C). Refractory materials offer the only possibility as structural materials. Tungsten alloys are attractive if some can be developed to operate under irradiation within a reasonable temperature window. Divertors in most recent design studies in the US and the EU for DEMO or power plants utilize a He-cooled W-alloy configuration to provide high-temperature operation. 'Making Tungsten Work,' the title of a recent paper at the ICFRM-14 [21], is a serious challenge that we need to understand and address. A recent paper by Tillack *et al* [22] summarizes development of divertors for a tokamak DEMO.

For first walls, the adoption of advanced ferritic steels as the structural material in many designs, such as the dual coolant lead lithium (DCLL) blanket favoured by the US, raises concerns due to the limited thermal conductivity and strength at high temperatures and one major limit for these designs will be the heat load to the first wall. The approach in most studies for power plants or DEMO reactors is to use a first wall that conforms to the shape of the plasma. As the ITER design has developed, the conforming first wall did not work due to the various constraints already in place in the designed structure and plasma control system. In the revised design, with revised heat loads for disruptions and ELMs, the first wall is made of shaped panels and the design heat load has risen from under 1 $\mathrm{MW\,m^{-2}}$ to ∼5 $\mathrm{MW\,m^{-2}}$ at the locations of maximum heat load. One expects that the improved understanding we are gaining from the research supporting ITER will lead to designs for DEMOs and power reactors that have effective means for managing the heat loads to their first walls, and that this will be a part of the next iteration of designs.

Liquid surfaces (see also section 6.2) offer the advantage that the surface is self-replenishing and therefore self-repairing, although there are also limits for the supporting structure. The liquid surface concepts fall into two categories: (1) fast flowing jets or troughs and (2) slow flowing surfaces, typically replenished through a porous medium with capillary forces. If the reactor concept has liquid surfaces for both the first wall and the divertor, then the long flow paths likely to be required for the first wall may present a more severe requirement than the high-heat load of the divertor for two reasons. First, the long flow path can lead to a high pressure drop due to MHD forces. Second, if the liquid is absorbing heat and not conducting much to a cooled substrate, then the integrated heat load along the flow path will limit the acceptable heat load.

Another requirement for developing high-heat-flux components for power plants is a credible development path. This aspect is less well explored, and is done usually by identifying the remaining issues as part of a design study, or by more comprehensively identifying and gaps, as was done in ReNeW [23]. The main point expanded below is that a credible development path implies that we explore the options for actively cooled high-temperature PFCs in several ways. One is the development and testing of materials, designs and fabrication methods that lead to confidence that we can build robust components. Another is the development of experiments that will show the effect of hot walls on the plasma. Plasma–surface interactions produce a complex non-linear feedback to the plasma. Hot walls present a new operating condition as yet unseen in fusion experiments. The interaction of the plasma with the walls includes many temperature-dependent processes (e.g. diffusion, absorption, recombination) that affect both incoming ion behaviour in the near-surface regions of the wall and also the longer term modification of the wall materials due to the combination of high temperature, ion bombardment and neutron irradiation. These issues are treated briefly in section 7.

The next point is extracted from the two above. A commitment to long-pulse hot-wall experiments in advance of a DEMO means at some point there is a deployment of actively cooled components over a large area of some new or upgraded confinement experiment. The introduction of any new technology into a confinement experiment represents a threat of new modes of failure. This in turn demands an adequate development programme for preparation and integration into the experimental programme of the chosen device.

Thus we should anticipate that progress towards adequate high-heat-flux components for applications such as DEMO must be preceded by progress in development of adequate materials and technology, e.g. helium-cooled PFCs with tungsten armour, and the preparation and deployment of material probes, experimental modules and component prototypes that will enable hot-wall experiments on one or more long-pulse high-power fusion experiments. Accompanying such activities will be the parallel development of adequate engineering diagnostics with which to evaluate the performance of these probes, modules, etc both for the protection of the experimental device and for the knowledge gained about the performance of the probes modules, etc

3. Physics of the edge: current understanding and projections to ITER and power plants

3.1. Fusion energy sciences joint facilities research target 2010: thermal transport in the scrape-off layer (SOL)

Beginning in 2008, the DOE Office of Fusion Energy Sciences asked the three major domestic fusion facilities Alcator C-Mod, DIII-D and NSTX to coordinate a yearly set of common experiments aimed at critical scientific questions that impact the extrapolability of results from present-day devices especially towards ITER. These specially focused experiments have become known as Joint Research Targets (JRT). For FY 2010, the JRT focuses on SOL transport, with the following wording:

'*Conduct experiments on major fusion facilities to improve understanding of the heat transport in the tokamak scrape-off layer (SOL) plasma, strengthening the basis for projecting divertor conditions in ITER. The divertor heat flux profiles and plasma characteristics in the tokamak scrape-off layer will be measured in multiple devices to investigate the underlying thermal transport processes. The unique characteristics of C-Mod, DIII-D, and NSTX will enable collection of data over a broad range of SOL and divertor parameters (e.g., normalized collisionality* ν^**, ratio of thermal to magnetic pressures* β*, parallel heat flux* $q_\parallel$ *along the magnetic field and divertor geometry). Coordinated experiments using common analysis methods will generate a data set that will be compared with theory and simulation.*'

In preparation for these experiments, all three devices commissioned and/or upgraded new diagnostics to measure the divertor heat flux with sufficient time resolution to separate steady and transient power loadings. The principal focus of the research plan at each facility is to obtain an accurate set of divertor heat-flux and plasma boundary layer profile measurements over the (wide) available range of externally controlled engineering parameters. Of particular interest is the dependence of the heat-flux width on plasma current, heating power, magnetic field and device size. Previous experiments have shown that the divertor heat-flux footprint narrows with plasma current, and depends only weakly on toroidal magnetic field and heating power when the SOL plasma outside the magnetic separatrix is in either the high particle recycling regime or the sheath-limited heat transport regime. The new experiments are aimed at confirming and extending those previous results for each regime. Divertor target heat-flux data were analysed using two-dimensional (2D) thermal analysis tools that compute surface heat flux from calibrated measurements of the increase in surface temperature. It is important to note that C-Mod operates with refractory metal divertor targets (Mo and W) in a 'closed' divertor shape (in which the divertor plasma is enclosed by walls to some extent) with a near vertical outer target; preliminary results were reported at the 19th International Plasma–Surface Interactions Conference, 24–29 May 2010, in San Diego [24, 25]. The DIII-D and NSTX divertors are operated in more 'open' geometries with less confinement of neutral particles. The DIII-D targets are horizontal ATJ graphite tiles [26, 27], while the NSTX targets are horizontal lithium-coated ATJ graphite tiles [28]. Additionally, the liquid lithium divertor (LLD) has just been installed in NSTX, so that part of its divertor target is now liquid Li. While the differences in the three machines' divertor geometries and materials may not affect the parallel heat conduction physics, they could affect the details of how the divertor heat flux is 'mapped' to the mid-plane, as well as the divertor detachment physics and the complexity of the infra-red (IR) emission measurements.

In addition, a set of coordinated experiments among the three facilities was conducted. These latter experiments allow the individual data sets to be joined together and compared directly over parameter ranges in which they overlap. These coordinated experiments were based on matching plasma physics dimensionless quantities ν^*, β and normalized ion gyroradius ρ^* in the plasma edge region. A true identity experiment also matches scaled shapes of the magnetic equilibrium (poloidal flux surfaces), e.g. elongation κ, triangularity δ, edge safety factor q_{95} and inverse aspect ratio $\varepsilon = a/R$, where a and R are the minor and major radii, respectively. A true identity experiment between C-Mod and DIII-D was executed since the aspect ratio can be matched, as achieved previously in a so-called pedestal similarity experiment [29]. The basic idea is to match these dimensionless parameters at the magnetic separatrix, and possibly at the top of the pedestal (several centimetres inside the separatrix), to determine whether the SOL profiles and scale lengths also match. Then scans about these points allow for scans of dimensionless parameters within each machine. Although NSTX has a different aspect ratio, it contributed to these coordinated experiments by running the same poloidal cross-section, i.e. an aspect ratio scan.

Theory and modelling of some of the key transport issues affecting the heat-flux widths were carried out in close concert with the experimental measurements. This includes turbulence simulations, neoclassical transport modelling and fluid transport modelling of varying complexity. Presentations on these on-going efforts were made at the April meetings

of the Edge Coordination Committee and the US Transport Task Force in Annapolis, MD. A number of theory papers were also presented at the 19th International Plasma–Surface Interactions Conference [30, 31].

A common feature in the experiments was the observation of an inverse dependence of the SOL heat-flux footprint on plasma current, I_p, with the weakest (strongest) dependence in Alcator C-Mod (NSTX). In addition, there was no clear dependence in all three devices on the TF B_t, or the power flow through the edge. Projecting forward to future devices, the main question is whether the observed unfavourable scaling with plasma current is offset by a favourable size scaling. In addition, additional research to develop very high flux expansion divertors, e.g. the 'snowflake' 'X', or 'Super-X' divertors, and to quantify the reduction in peak heat flux, is needed for projection.

All four of the quarterly status reports for the 2010 JRT are available at the DOE OFES website at www.science.doe.gov/ofes/performancetargets.shtml.

3.2. QH-mode and ELM-free regimes

Overview. ELM control is one of the most challenging requirements for the compatibility of a core thermonuclear plasma with acceptable plasma edge conditions. The large type-I ELMs occurring in conventional H-mode discharges can result in large particle and heat fluxes to the divertor. Both ELM-free and small ELM regimes have also been found under certain discharge conditions that significantly mitigate the divertor load. However, these regimes are currently restricted to fairly narrow operational ranges. The most promising of the ELM-free regimes appear to be the quiescent-H-mode (QH-mode) and RMP discharges. Both are associated with the presence of non-axisymmetric fields (external in the case of the RMP discharges and generated by a plasma MHD mode in the QH-mode), accompanied by a density reduction or pump-out. Regimes with small ELMs tend to appear for defined regions of triangularity, δ, q_{95} and proximity to double null (DN) and are not observed in all tokamaks. The most reactor-relevant of these appears to be the type-II regime, though shaping can be used to some extent.

Quiescent H-modes. This operational regime was first observed in DIII-D and more recently has been reproduced in JT-60U, ASDEX-U and JET. QH-modes operate ELM-free with constant density and radiated power for long duration (>4 s or $30\tau_E$), limited only by hardware constraints [32]. However, while they exhibit H-mode confinement improvement, they are mostly lower to moderate performance discharges with the pressure pedestal usually somewhat lower than conventional ELMing H-mode. QH-mode is seen over a large range of input power in DIII-D, from 3 to 15 MW, limited by the core beta limit. QH-mode plasmas operate at or near the peeling boundary, in contrast to conventional type-I ELMing H-mode, which typically operates near the convergence of the peeling and ballooning stability boundaries. Initially only obtained in discharges with rotation counter to the current, it has recently been extended to co-rotation in DIII-D [33].

ELM-free operation is associated with the presence of continuous, rotating MHD modes, the edge harmonic oscillation (EHO) in the pedestal region. This mode appears to be associated with the density pump-out, which allows transport equilibrium to be established at edge conditions near but below the peeling–ballooning stability limit and also facilitates He ash exhaust. The EHO is a saturated low-n peeling–ballooning mode destabilized by rotational shear just before edge plasma reaches the zero-rotation stability boundary.

A major restriction is that there is a minimum pedestal velocity shear necessary for QH-mode and so QH-modes required significant torque, usually supplied by neutral beam injection (NBI). However, recently, it was found that static $n = 3$ non-resonant magnetic fields (NRMFs) provide a new knob to change the pedestal velocity shear, thereby allowing sustained QH-mode with zero net NBI torque [34]. There are additional advantages to using NRMFs, including improved resilience to error field penetration and inhibition of destabilization of neoclassical tearing modes.

Applied RMPs. ELM suppression and ELM-free operation have also been reproducibly observed in DIII-D with an applied $n = 3$ RMP from external non-axisymmetric coils [35]. In general, there is a significant reduction in the pedestal electron density. Suppression is obtained for resonant q_{95} values in the range $3.4 < q_{95} < 3.7$ and also for $7.0 < q_{95} < 7.2$, for $1.4 < \beta_N < 2.4$, $5 < P_{inj} < 15$ MW, and for various shapes ranging from a lower single null (LSN) with low and high triangularity, δ, and for near DN discharges at high δ.

The ELM-suppressed RMP discharges have mostly lower to moderate performance and pedestal than conventional ELMing H-mode. The physics responsible is currently not well understood. Peeling–ballooning stability analysis shows that the RMP generally suppresses ELMs by moving the operating point into the stable region. Suppression is apparently not due to ergodic fields since the plasma response appears to shield the external vacuum field except in a small region at the edge. ELM suppression seems to be related to stopping continual penetration of the edge pedestal. The cause of this is unknown. RMP ELM suppression or mitigation has also been observed in JET and MAST. Coil upgrades are planned on ASDEX-U, NSTX, DIII-D, JET, ITER and MAST to investigate the physics of RMPs and the effect on ELMs.

Type-II ELMs. Type II is a small ELM regime observed in JT-60 and occasionally in DIII-D, ASDEX-U and JET. Also, a new 'type-V' regime in NSTX has many similarities to the type-II ELMs in other devices. Generally, the onset of type-II or 'grassy' ELMs requires strong shaping ($\kappa > 1.8$, $\delta > 0.3$), low current, low rotation and low collisionality with $\nu^* < 1$ [36]. The high ELM frequency, up to ~kHz, yields low heat loads on the divertor. However, they are not reliably reproducible and provide mostly lower to moderate performance with a pedestal usually lower than conventional ELMing H-mode. The direction of toroidal rotation seems to be important rather than the rotation shear.

Other regimes. The enhanced D-alpha regime observed in Alcator C-Mod [15] shares some similarities to the QH-mode in that it is ELM-free and associated with the presence of a continuous saturated MHD mode, although the quasi-coherent mode (QCM) in C-Mod is at a much higher frequency than the EHO. The regime has not been reproduced reliably however in

any other machine, though a similar mode has been observed on JET. The onset appears to be restricted to intermediate δ and q_{95}, with $0.3 < \delta < 0.55$ and $3.5 < q_{95} < 4$. It apparently requires increased recycling and is observed only with ICRH. In contrast to other ELM-free regimes, the baseline D_α signal actually increases but confinement improves and high pedestal gradients are obtained, typically larger than those in conventional H-mode, and correspondingly improved performance.

An improved L-mode (I-mode) has also been observed in Alcator C-mod, in which there is a H-mode pedestal on the temperature profile, but not on the density profile. The overall performance still gives $H_{98y2} \sim 1$ at $\nu_e^* \sim 0.1$ [37]. The regime requires unfavourable ∇B drift. There is no particle barrier and no impurity accumulation. I-mode is also associated with 100–200 kHz density and field fluctuations. These may inhibit formation of the particle transport barrier.

The quasi-stationary, ELM-free H-Mode (QSEFHM) was observed with intense third harmonic X-mode ECRH and no NBI in TCV [38]. The QSEFHM phase lasts about ten energy confinement times with very good confinement: $H_{98y2} \sim 1.4$. Electron pressure profiles are very similar to those in the type-I ELMy phase. A key restriction, however, is that the modification of the edge profiles by heating and current drive may not scale well to reactor conditions.

In NSTX, discharges with Li conditioning have been found to range from ELMing to infrequent ELMs to ELM-free discharges, depending on the level of Li conditioning [39]. The Li is injected from overhead Li evaporators between shots. Fully ELM-free operation apparently requires massive amounts of Li. The physics responsible is unknown but the change in the density profile from Li injection is thought to be the first step to ELM suppression. The key issue is the observed impurity accumulation during ELM-free operation.

The type-III small ELM regime has been observed in several tokamaks. This regime occurs only at low T_e, near the H-mode threshold and is generally associated with reduced confinement. A precursor is usually observed that is more coherent than the precursors for type-I ELMs; this is thought to be due to resistive instability. The pressure threshold can be near type-I values since $T_e \sim 1/n_e$. Typically, the ELM frequency decreases with increased heating and the type-III ELMs disappear as the H-mode threshold is significantly exceeded and type-I ELMing ensues. For this reason, the type-III regime is not thought to scale well with reactor conditions.

Using detailed cross-section shaping changes, and in particular strong outboard squareness, the size and frequency of ELMs can be controlled to some extent. The physics is fairly well understood in terms of the shape changes modifying the field line connection length in the outboard bad curvature region. However, the major drawback is that the performance is usually degraded since the more unstable higher n modes limit the pedestal gradients to lower values.

Conclusions. Many open issues remain in extending the several small ELM and ELM-free regimes to reactor conditions. Each regime has several conditions that restrict operation and may be incompatible with other reactor requirements. The essential physics of ELM-free and small ELM regimes needs to be understood and the required conditions need to be determined more precisely for each regime since the present operational range of conditions is relatively narrow.

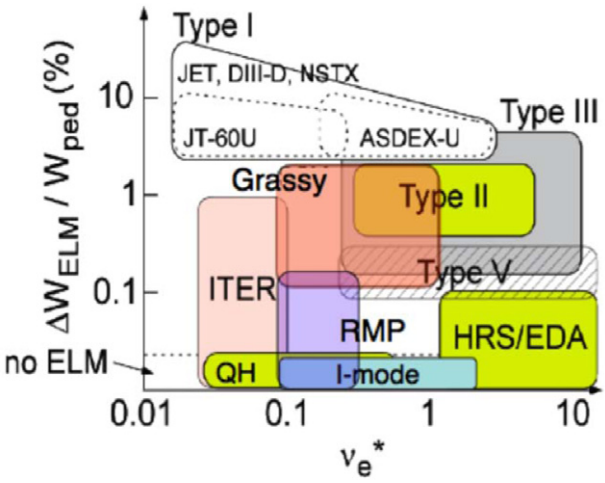

Figure 2. ELM-free and small ELM parameter spaces.

Figure 2 summarizes the ELM-free and small ELM regimes overlaid in the parameter space of collisionality versus ELM energy and compared with the conventional type-I ELM regime as well as the position ITER intends to operate in. The Li-conditioning regime is not shown since it depends apparently less on the plasma conditions than on the Li injected from outside. From the figure, it would appear that the QH-mode and RMP options are most relevant to low collisionality operation. Nevertheless, if the conditions can be expanded in the other cases, these could be reactor relevant as well and so should not be dismissed.

4. Modelling of the tokamak edge

4.1. Power exhaust simulation for the SlimCS divertor with the SONIC code

SlimCS is a conceptual DEMO design of a low aspect ratio tokamak ($R/a = 2.6$) with a reduced-size central solenoid coil for steady-state operation with core dimension similar to those in ITER, power generation capability of a gigawatt level, and taking into account economical prospect towards commercialization. The poloidal cross-section of the plasma and the first wall is shown in figure 3 [40]. For fusion power of $P_{fus} \sim 3$ GW, a total heating power of $P_{heat} \sim 600$ MW and $P_{out} \sim 500$ MW are expected. Thus, the power exhausted to the SOL is 5–6 times larger while R is smaller than that of ITER. For the development of the plasma operational scenario, a total radiation loss fraction (P_{rad}^{tot}/P_{out}) of more than 90% is required in the edge and divertor. From the engineering design point of view, the appropriate choice for the PFC, SM and cooling system is more restricted than for ITER, under the condition of significant neutron irradiation and high operation temperature. At this stage, the power handling requirement of a divertor design with tungsten-PFC, RAFMS-SM and pressurized water cooling is expected to be 7 MW m^{-2}, which is lower than that in ITER. Power handling through a combination of plasma operation, divertor design and divertor engineering is a very important issue for the reactor design.

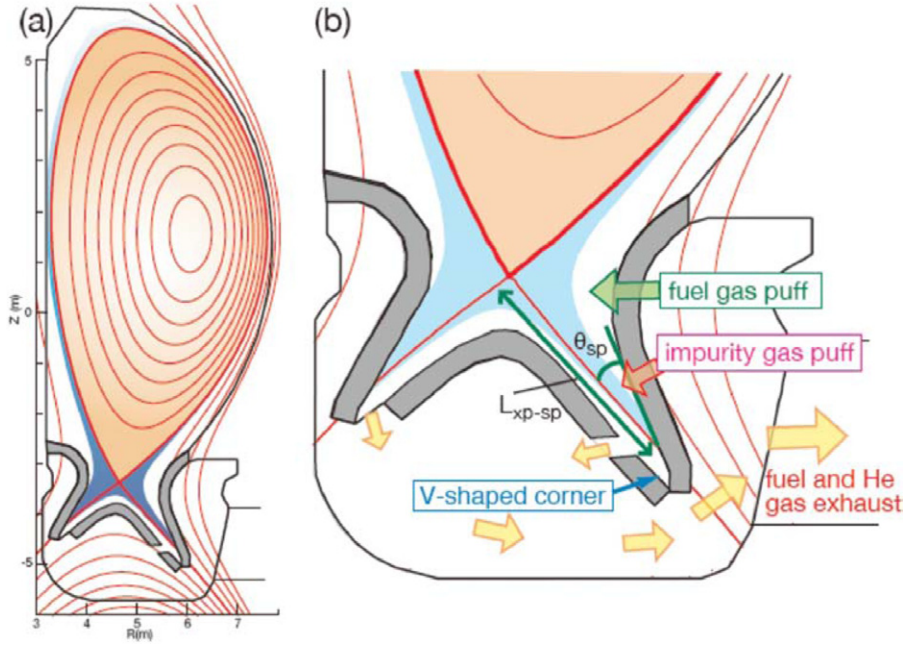

Figure 3. (*a*) Cross-section of the SlimCS plasma configuration and the first wall. (*b*) Illustration of the plasma configuration and the divertor geometry.

A divertor geometry, SlimCS, was proposed in [41], and the basic design concept for the ITER divertor, i.e. formation and control of detachment of the divertor plasma, is applied. At the same time, in order to reduce the peak heat load, the effects of the divertor geometry on the power and particle handling are enhanced: (1) the divertor leg is longer (inner $L_{\text{xp-sp}} = 1.37$ m, outer $L_{\text{xp-sp}} = 1.83$ m) and the inclination of the target (poloidal angle: inner $\theta_{\text{sp}} = 21^\circ$, outer $\theta_{\text{sp}} = 18^\circ$) is larger than that in ITER to increase particle recycling and radiation power efficiently along the divertor leg, (2) a private dome is installed to increase the neutral pressure for the exhaust of tritium gas and helium ash from the private flux region, (3) the outer exhaust slot is located above the bottom of the divertor, which will efficiently produce plasma detachment near the strike-point in the V-shaped corner. At the same time, intense impurity seeding is required to increase the radiation loss in the plasma edge and divertor.

Plasma simulation has been performed for the SlimCS divertor design. Formation of the divertor detachment ($T_{\text{e}} \sim$ a few eV) and the radiation distribution over a wide range in the edge, SOL and divertor are key issues for handling the huge power. For the first divertor simulation [41], the SOLDOR/NEUT2D codes were used assuming concentration of the seeding impurity with a non-coronal radiation model [42]; effects of the divertor geometry and Ar seeding on the target heat load were investigated. In order to reduce the serious heat load at the outer target, the radiated power in the outer divertor was increased by increasing the ratio of $n_{\text{Ar}}/n_{\text{i}}$ from 2% to 5%, while a constant value of $n_{\text{Ar}}/n_{\text{i}} = 1\%$ was set in the inner divertor and edge regions. Here, the radiation power function of Ar ions is less sensitive to the electron temperature range between a few 10 and a few 100 eV, compared with that of lower Z gases such as Ne and N_2, which have a peak at 20–50 eV [42]. Figure 4 shows a summary of the previous work; case-3 with a V-shaped corner with

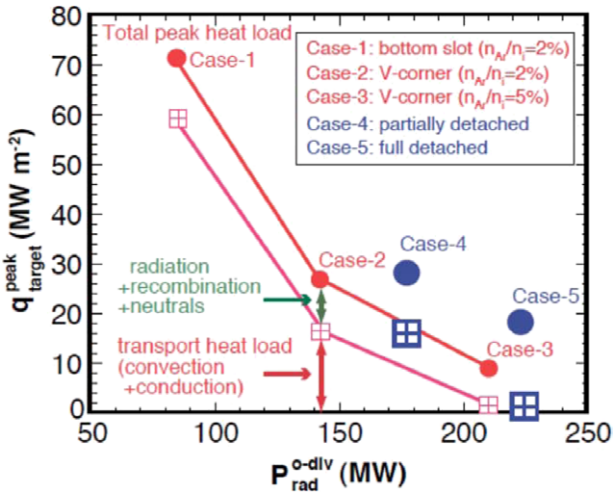

Figure 4. Peak heat loading at the outer target, $q_{\text{target}}^{\text{peak}}$, as a function of total radiation power in the outer divertor, $P_{\text{rad}}^{\text{o-div}}$, for the SONIC results [43] (case-4 and case-5) shown by large circles and squares, in addition to the SOLDOR/NEUT2D results (case-1, -2 and -3 [41]).

$n_{\text{Ar}}/n_{\text{i}} \sim 5\%$ at the outer divertor can produce a fully detached divertor, where $P_{\text{rad}}^{\text{div}}$ at the outer divertor ($P_{\text{rad}}^{\text{o-div}}$) increases to 210 MW, and $P_{\text{rad}}^{\text{div}}/P_{\text{out}} \sim 66\%$ and $P_{\text{rad}}^{\text{tot}}/P_{\text{out}} \sim 92\%$. The peak heat load is reduced to $q_{\text{target}} \sim 9\,\text{MW m}^{-2}$, which is attributed mostly to power loading by radiated power and neutral flux, compared with the convection and conduction heat fluxes (the plasma transport term). It was found that the distribution of the radiation loss over a wide area in the edge and divertor is very important in order to avoid local overheating of the PFCs.

For the recent study [43], transport of Ar impurity was investigated in the SONIC code [4], using a Monte Carlo simulation (IMPMC), which has advantages for impurity

modelling since most kinetic effects on the impurity ions such as forces produced by temperature gradient and flow of the background ions along the magnetic field are incorporated into the original formula. In the first stage, Ar transport and plasma evolution were self-consistently simulated up to a typical transport timescale in the divertor such as $t = 100$ ms, for two different initial conditions, namely partially and fully detached divertor plasmas (case-4 and case-5. respectively). Figure 4 also shows $q_{\rm target}$ for the two cases. Here, the Ar density and its concentration are increased and their peaks are localized near the target, compared with those in case-2 and case-3. This is produced by the intense friction force on the impurities, while the effect of the thermal force was within rather narrow flux surfaces near the separatrix. The influence of enhancement of both $n_{\rm e}$ and $n_{\rm Ar}$ on the peak heat load becomes significant; in the fully detached divertor (case-5), $q_{\rm target} = 18\,{\rm MW\,m^{-2}}$ is attributed to the radiation power load, which is twice as large as case-3, whereas $P_{\rm rad}^{\rm o\text{-}div} = 223\,{\rm MW}$ is slightly larger. Note that the self-consistent solutions of the plasma, neutrals and impurity are still transient in the upstream divertor, SOL and edge. Further extension of the simulation up to the particle confinement time, of the order of a second, will be required to obtain impurity and radiation distributions by Ar ions with higher charge states.

In summary, in the development of the self-consistent divertor simulation, SONIC results with Ar seeding showed that radiation power loading was enhanced due to the localization of the impurity above the target. Thus, in order to avoid local overheating of the PFCs, distribution of the radiation loss over a wide area, i.e. edge and divertor, should be established for example by improving the divertor geometry appropriate for full detachment, determining an appropriate radiator, or a combination of the two.

For future DEMO divertor design, a SONIC simulation has been developed to improve the design for particle control in order to satisfy helium exhaust, as well as maintaining the divertor detachment in the high neutral pressure and radiation loss: development of SONIC with multi-species (Ar and He) Monte Carlo (MC) simulations started. Thermal stability of the divertor plasma with seeding and metallic (high-Z) impurities should be investigated. At the same time, understanding of physics processes and improvement in the modelling under the ITER/DEMO-level high flux density is required, such as atomic–molecular–impurity processes (n–n/i–n collision, photon absorption, molecular assisted recombination).

For the development of integrated simulation codes extending to the steady-state level ($t \sim 1$s), a parallel computer with an effective speed of 100 TFlops (5000 times faster than JAEA: 20 GFlops) such as the IFERC-level will be required to reduce the SONIC calculation from ∼9 h run time (for 10 ms solution) to 0.2 h for the steady-state (1 s) solution.

4.2. UEDGE, edge turbulence and kinetic effects

The numerical simulation of plasma exhaust to project the distribution of particle and heat fluxes to PFCs is currently done mainly using 2D plasma transport codes where the tokamak magnetic field ($\boldsymbol{B}$), plasma and walls are assumed to be toroidally symmetric. There are such activities in the US, Europe, Japan and elsewhere. Here we describe the models used in the UEDGE code [44, 45] and some related extensions.

UEDGE is a multi-species fluid transport code that simulates plasma, neutral and photon transport in the tokamak boundary region from several centimetres inside the magnetic separatrix to material surfaces outside the separatrix. This region thus encompasses what is typically referred to as the plasma edge just inside the separatrix and the SOL outside the separatrix. The computational mesh is based on the detailed magnetic equilibrium with toroidal and poloidal magnetic fields as obtained from an MHD equilibrium code such as EFIT [46]. A body-fitting non-orthogonal algorithm is used to approximately fit the mesh to the geometry of the divertor plates, while much of the main chamber is usually approximated as an outer poloidal magnetic flux surface. However, UEDGE has the capability to extend the mesh beyond the secondary separatrix for a nominally single-null configuration such as ITER, and thus can model the details of plasma/wall interactions in the vicinity of the secondary magnetic X-point [47]. The plasma transport is taken to be classical along the magnetic field [48] with the addition of flux limits for kinetic corrections. The transport across the magnetic field is described by enhanced diffusion and convection coefficients to represent plasma turbulence that is believed to generally dominate collisional transport. UEDGE also includes the option to model classical cross-magnetic-field drifts associated with $\boldsymbol{E} \times \boldsymbol{B}/B^2$ and gradient-B/curvature drifts that can be compared with anomalous plasma fluxes, especially for steep radial gradients encountered in the enhanced-confinement H-mode regimes [49].

In addition to hydrogenic species, UEDGE also simulates impurity species by following the separate charge-state ions, e.g. native carbon, beryllium or tungsten as well as neon, and other similar species injected to enhance radiative loss in the edge region. The sputtering of PFC material as an impurity source is included via yield curves that include physical and chemical sputter rates. The line radiation energy loss is removed from the electron channel and its projected heat-flux contribution to PFC surfaces computed. Impurity radiation is assumed to be optically thin, whereas trapping of hydrogen radiation is included via an escape-factor model calibrated with a radiation transport code [50]. The neutral species is usually represented as fully dynamical fluid species where particle and energy fluxes are limited to thermal streaming values based on a comparison with more detailed MC neutral simulations. To properly utilize the fluid model, an accurate non-orthogonal (at least nine-point) difference stencil must be used. Direct coupling to MC neutrals is implemented, but the option is seldom used. The basic UEDGE models described have been used extensively to model edge plasma characteristics and wall fluxes for a number of existing tokamaks, e.g. DIII-D [51], NSTX [52], Alcator C-Mod [53] and JT60-U [54] as well as ITER [47] and some ARIES designs [44].

A number of enhancements have been developed to strengthen the realism and predictive capability of edge modelling. An important shortcoming is the determination of the enhanced radial plasma transport coefficients; these are usually determined by adjusting spatially dependent values such that radial mid-plane plasma profiles fit experimental data (an interpretive approach) and then using the same coefficients to project the characteristics for future devices. To overcome this problem, a method has been developed to couple UEDGE

Table 2. Summary of edge physics and related codes mentioned in the text.

Code name	Description	References
UEDGE	2D multi-species fluid pedestal/SOL transport for plasma/neutrals with wall recycling and sputtering	[44, 45]
EFIT	MHD equilibrium	[46]
BOUT	3D non-linear electromagnetic fluid code used to study turbulence and transport in the pedestal and SOL, as well as ELM dynamics	[55]
WBC	Sheath/SOL MC impurity ion transport	[56]
WallPSI	1D multi-species surface recycling/sputtering and transport within the wall material	[57]
TEMPEST	Continuum 4D kinetic edge transport with collisions and anomalous kinetic diagonal transport matrix model with velocity-dependent convection and diffusion coefficients	[60]
COGENT	Continuum 4D kinetic edge transport with improved models and numerics; second generation TEMPEST	[62]
XGC0	Particle-in-cell 4D kinetic edge transport	[61]
EPED	0D model which combines peeling–ballooning and kinetic ballooning mode stability tests to predict pedestal height and width	[93]
SOLT	2D non-linear electrostatic fluid code used to study turbulence and transport in the pedestal and SOL	[95]
ESEL	2D non-linear electrostatic fluid code used to study turbulence and transport in the pedestal and SOL	[97]

with the edge/SOL 3D turbulence code BOUT [55] that allows fluctuations to have toroidal variations. Here plasma fluxes and profiles are exchanged between the two codes to obtain a consistent steady state. The transport coefficients are similar to those deduced from the interpretive modelling, but the method allows more reliable projection to future devices.

Refined models of PMI and associated material migration for UEDGE simulations are included by coupling either to the near-surface MC impurity ion code WBC [56] or to the WallPSI code [57], which is a component along with UEDGE of the FACETS project [58]. An example of the coupling to WBC is given in [56] for the migration of beryllium from the main chamber of ITER to the divertor surfaces. The FACETS project is a US SciDAC collaboration to develop a whole-device model that initially couples core and edge/SOL transport components together with the one-dimensional (1D) WallPSI model that gives a time-dependent hydrogenic wall neutral source from recycling and impurity neutral wall source from sputtering. In addition, WallPSI computes the transport and retention of hydrogen within the material as well as the temperature within the material.

The final model extension discussed is that of kinetic effects that go beyond the strongly collision/diffusive models considered so far, and are especially important to fully evaluate hot edge plasmas of future devices. Such a model goes well beyond UEDGE and is much more than a simple extension. Here the ion and electron particle distribution functions are not assumed to be close to Maxwellian but are rather solved for from the 4D kinetic equation where the two added dimensions are those of velocity. The third velocity dimension of gyrophase is averaged over with varying degrees of sophistication. There are two types of effects captured by the kinetic codes, the first being large mean free path distortion of the distribution function along the magnetic field (parallel direction). As a consequence, the parallel thermal conductivities and thermal force terms can be reduced [59], which in fluid models is approximated by flux limits. The second type of kinetic effect is the appearance of large drift (neoclassical) orbits whose radial extent is much larger than the particle gyro-orbits owing to the toroidal geometry. Such orbits can enhance the radial collisional transport, especially for ions. This capability for edge plasmas is being developed both using a mesh-based continuum method for the distribution function for the TEMPEST and follow-on COGENT codes [60] and a particle-in-cell method for the XGC0 code [61]. Both of these methods are also being extended to 5D by including toroidal fluctuations, thereby yielding the kinetic equivalent of the 3D fluid BOUT turbulence code.

Table 2 summarizes the edge physics and related codes that are mentioned in this section, together with a brief description and references to more detailed explanations.

4.3. Neutral transport from wall to SOL

The material surfaces surrounding a fusion device act as sinks for plasma particles, momentum and energy as impinging electrons and ions recombine when they strike the surface. They are not, however, sinks for mass [63]. The associated PMIs yield neutral hydrogen atoms and molecules that travel freely across field lines and are ionized in the plasma volume. Through this recycling process, the plasma can refuel itself. These PMI can also result in neutral impurity atoms or molecules by physical or chemical sputtering. The basic concepts underlying these processes [64] are the same for present-day experiments, ITER and power producing reactors. However, the details of the edge and divertor plasmas in these three regimes will differ dramatically.

The primary differences are associated with the state of the material surfaces. The representations of materials used to model PMI in most current codes are relatively simple and are not representative of the actual plasma-facing surfaces in tokamaks. The latter are complex 'self-consistent' material surfaces that are the result of the long-term effects of plasma impact, erosion and redeposition. Not only are we unable to model this material state, the high fluences found in present-day tokamaks cannot be easily replicated in small-scale experiments that would be easier to diagnose. Work on improved models that can better characterize such surfaces and simulate their temporal evolution is underway [57, 65], as is the development of more fundamental, nearly first-principles approaches that may be able to describe them

comprehensively. Testing these models will require better and more PMI diagnostics in tokamaks, as well as more capable test stand experiments [23]. Experiments and model development to prepare for the PMI challenges that ITER will bring have begun; these efforts are targeted at its unique combination of materials, high-heat and particle fluxes, and long-pulse lengths. The step to power plant regimes will require even greater extrapolation from the present database, bringing in higher wall temperatures, heat and particle fluxes. A substantial R&D effort will be needed to develop and test models capable of predicting material behaviour and PMI under these conditions.

The transport of PMI-generated neutral atoms and molecules into the plasma is governed primarily by their interactions with the plasma ions and electrons. The two most fundamental processes for hydrogen atoms, electron impact ionization and charge exchange/elastic scattering, are relatively well understood [66, 67]; these models are applicable to all envisioned plasma regimes. The development of correspondingly detailed models for impurity atoms continues to work its way up through the periodic table. Those for lighter species (e.g. Li [68], Be [69]) are in hand; one for carbon is nearly complete. However, handling the vastly more complicated level structures of high-Z atoms, such as Mo or W, favoured for reactor plasma-facing materials in a computationally tractable way will require the use of approximate models that are still able to reproduce their radiation and ionization characteristics with acceptable accuracy.

The basic set of processes describing the ionization and breakup of hydrogen molecules [70] sufficed for the low-density limiter and divertor SOL plasmas of 20 years ago. However, the higher plasma densities and lower temperature attained in some present-day divertors, also expected for ITER and subsequent devices, result in longer lifetimes for molecular species and, thus, additional processes. In particular, vibrational excitation becomes significant under these conditions, bringing other processes, such as ion conversion, and additional species (e.g. H^{+3} and H^-) into the problem [71]. A practical but approximate model that treats these vibrationally excited states as short-lived is being used in the design of the ITER divertor [72]. However, the validity of this approximation in the extrapolation to reactor conditions will have to be established by testing against a more detailed model in which these vibrationally excited states have lifetimes comparable to transport timescales [73]. The basic data describing the breakup of hydrocarbon molecules are on a much firmer footing than was the case a decade ago [74, 75], and possible approaches to dealing with the complexity of their penetration into the plasma are being investigated [76]. These data are needed to validate models of impurity behaviour in present-day devices, but are of less interest for ITER and subsequent devices due to concerns with tritium retention in the presence of carbon PFCs. Instead, an effort to understand the molecular species pertinent to those edge plasmas will be needed.

The high plasma densities and low temperatures in the ITER divertor are required to achieve a partially detached state that allows 60–70% of the power flowing into the divertor to be carried away by photons and neutrals [77] and spread over a larger area. Otherwise, the heat loads and associated erosion of the divertor target plates would lead to unacceptably short material lifetimes. The even higher heat and particle fluxes in a reactor regime will place yet greater demands on the efficiency of these heat removal processes, and on our understanding of them to permit the development of suitable designs. In a detached divertor, the plasma travelling down the SOL loses much of its energy and momentum prior to reaching the target plate. The principal experimental signature is a target flux that decreases with increasing upstream density. The number and complexity of processes potentially involved in detachment, including charge exchange/elastic scattering and volume recombination, is great enough that there may in fact be more than one type of detachment [63]. Consequently, simulating detachment in edge plasma modelling codes has been challenging [78]. Fully replicating the observed behaviour may require models closer to first principles than those in hand. Corresponding improvements in diagnostic data will be required to motivate and validate these models.

Neutral–neutral elastic scattering of H and H_2 is significant under these high-density conditions [72], as is trapping of Lyman-α radiation by H atoms [79]. An approximate technique for handling the non-linearity introduced by the former suffices. However, simulating the latter requires self-consistently treating the interactions between the plasma, gas and radiation fields, as well as incorporating the various phenomena that determine the emission line shape (Doppler and Stark broadening, Zeeman splitting, etc) [73]. The most comprehensive model currently in use exploits the analogies between photon and neutral transport, allowing both to be simulated within the same MC framework [73]. The high opacity found in detached divertors may allow the use of an alternative, more approximate treatment [80]. The development of these models will proceed in parallel with those of plasma detachment.

The models used to describe PMI are a primary source of uncertainty in existing kinetic neutral transport models, as was explained above. Plasma transport models are another. Kinetic plasma turbulence and transport codes are being developed and coupled with kinetic neutral transport routines (see, e.g., [81]) to provide a much closer to first-principles simulation capability. These codes will mature over the next several years and be validated against existing experiments.

5. Experimental benchmarking of models for power plants

5.1. Introduction

The benchmarking of models for the plasma edge and PMI is critical to the prediction of the associated behaviour at the reactor regime with large particle and power loads, long plasma durations, and limited material lifetimes. Models exist for describing the (1) SOL plasma, (2) neutrals, (3) impurities, (4) wall interactions and also the (5) pedestal/edge plasma. The fidelity of these physics models varies widely, and there are ongoing programmes around the world to develop more sophisticated and complete models utilizing the highest performance computing platforms. Some benchmarking activities have been performed. These normally examine

separate components or pairs of components listed above, and have shown reasonable trends. However, it is clear that the state of the model to experimental comparison in this area is immature compared with that in the core plasma, due to both a lack of detailed diagnostics and focused efforts in comparisons between models and experiments.

Benchmarking exercises breakdown into specific components, (1) what is being compared (scalars, profiles, fluctuations), (2) what is the diagnostic information available for comparison, (3) what is the structure for modelling, experimental comparison and model improvement. ITER has provided an important focus to the modelling of edge plasmas and PMI, and in order to make progress in the design of the device, has developed correlations relating experimental results to primary parameters of interest, such as the first wall and divertor heat and particle fluxes under nominal and transient conditions. ITER has also utilized the B2-Eirene combination (2D edge plasma model and neutrals module) to solve for the consistent divertor and plasma separatrix conditions. These allow the identification of acceptable operating windows, for example, for heat flux on the divertor and He concentration at the plasma separatrix.

The following questions arise: what will be different in the reactor regime compared with present experiments and ITER? Are there fundamental edge plasma parameter changes like the ρ^* parameter in core plasma physics? Is it simply that the heat and particle fluxes will be higher? A power plant will likely produce only a single main operating configuration that has been optimized, apart from some fractional power states required to start the device up. A significant effort has been made with modelling to identify edge plasma regimes of operation that are acceptable for ITER, but techniques to control these regimes seem less well developed. Can we envision the control required for the reactor regime, and how can they be tested on near-term devices? Ultimately the modelling capability must allow moving from physics description to design criteria, in a similar vein as ITER has tried to do.

The reactor environment, or even approaching the reactor environment, may make diagnosing edge plasmas and material interfaces very difficult, and so it appears that we have a shrinking window for verification of sophisticated physics models. Can we verify the physics models in pre-nuclear devices and low fluence environments like ITER, and use the models to extrapolate to the reactor regime?

The benchmarking of these physics models for the reactor regime raises a series of critical issues:

(1) What is the reactor environment, or a reasonable approximation of that environment?
(2) What are the most critical parameters in the reactor?
(3) Benchmarking involves comparisons at accessible regimes, which is then used to make projections to the reactor regimes.
(4) The ultimate goal is actual integration of the core and edge plasmas, and the material wall.
(5) Edge plasma and material surface diagnostics development is critical to progress in this area.
(6) What diagnostics can be used in the reactor regime?

5.2. Progress in validating predictive transport models

It is now widely recognized within the fusion community that the development of validated modelling capabilities is essential for predicting the performance of ITER and other future experiments with a high degree of confidence. A number of results presented at the meeting highlighted the great progress that has been made in developing first-principles-based transport and confinement models, which can be used to predict characteristics of both the core and edge regions of a plasma. While these regions are generally modelled separately, recent efforts within two of the 'proto-FSP' SciDAC projects have begun to address how they can be self-consistently coupled.

Although not the explicit focus of this workshop, a summary of recent core turbulent transport modelling results was presented, with an emphasis on the various validation studies of these models. As an example of a validation 'best practice', comparisons of transport solutions (i.e. steady-state density and temperature profiles) predicted by the quasilinear trapped gyro-Landau fluid (TGLF) model [82, 83] against a database of 96 experimental discharges spanning multiple machines and confinement regimes was presented. Model fidelity was assessed using community-designed metrics [84] based on the incremental stored energy $W_{\rm inc}$ (the energy stored above the $\rho = 0.84$ boundary condition), finding that $\langle R_{\rm Winc}\rangle = \frac{1}{N}\sum_i (W_{si}/W_{xi}) = 1.02\%$ and $\Delta R_{W_{\rm inc}} = \sqrt{\frac{1}{N}\sum_i (W_{si}/W_{xi}-1)^2} = 19\%$, where i is a discharge index, and W_{si} and W_{xi} are the simulation and experimental incremental energies, respectively. In contrast, benchmarking the GLF23 model [85] (TGLF's predecessor) against the same database yields 'scores' of $\langle R_{W_{\rm inc}}\rangle = 1.16\%$ and $\Delta R_{W_{\rm inc}} = 36\%$. In parallel to these advances in reduced transport models, there are now multiple transport solvers [86, 87] that can couple fluxes calculated by non-linear gyrokinetic simulations from the GYRO [88] and GS2 [89] codes to predict steady-state core profiles. Using these non-linear simulations, one can not only predict equilibrium profiles, but also self-consistent fluctuation characteristics which can then be directly compared with experimental measurements to obtain a much more fundamental testing of the underlying gyrokinetic formalism. It is important to note that such comparisons, whether in the core or edge, generally require the use of detailed synthetic diagnostics [90] that account for, e.g., spatiotemporal sensitivities of a specific diagnostic. (A 'synthetic diagnostic' applies a known instrumental response to the output of a computer model to predict the signals that should be observed by a real experimental diagnostic.)

A key limitation of these current core transport models is that they require a boundary condition that specifies plasma conditions at some outer radius, nominally the 'top' of the edge pedestal region. Self-consistent prediction of this boundary condition requires validated models of both ELM stability (which provide a hard upper limit on the pedestal height and width), and edge turbulence, which regulates the pedestal structure in the absence of ELMs. Both topics have seen significant progress in our understanding and predictive capability.

One of the most encouraging advances in our understanding of pedestal physics has been the successful

Table 3. Summary of core transport physics codes mentioned in the text.

Code name	Description	References
GLF23	Quasilinear gyrofluid model, able to calculate linear growth rates and mode structures, and to combine those with saturation rules to predict turbulent fluxes	[85]
TGLF	Quasilinear gyrofluid drift-wave instability and transport model; second generation of GLF23 approach with increased physics fidelity for effects such as trapped particles, plasma shaping, rotation, collisionality, etc	[82, 83]
GYRO	Non-linear 5D continuum gyrokinetic δf simulation, used to predict turbulence and transport levels self-consistently for given (input) equilibrium profiles	[88]
GS2	Non-linear 5D continuum gyrokinetic δf simulation, used to predict turbulence and transport levels self-consistently for given (input) equilibrium profiles	[89]

development and validation of a model for predicting the onset of type-I ELMs, which drive the largest heat and particle fluxes to the wall and divertor, in terms of a peeling–ballooning stability limit [91, 92]. The peeling–ballooning instability is an intermediate toroidal mode number ($n \sim 3$–30) MHD instability that leads to a constraint on the pedestal height as a function of width. More recently, the EPED1 model [93] has been developed, which combines the peeling–ballooning limit with a second constraint based on the onset of kinetic ballooning modes (KBM), which are believed to drive very stiff transport once they become unstable [94]. Combining the peeling–ballooning and KBM constraints allows prediction of the two unknowns: the pedestal height and width. Testing of the model against a variety of discharges from multiple machines yields good agreement with measurements, with a comparison to 20 discharges (6 Alcator C-Mod, 7 JET and 7 DIII-D) yielding a ratio of predicted to observed pedestal heights equal to 1.02 ± 0.2.

Modelling of edge and SOL plasma turbulence and transport via non-linear fluid simulations has also advanced significantly in recent years. A good representative of this class of work is the scrape-off-layer turbulence (SOLT) code of Russell *et al* [95]. The code uses a 2D fluid representation to evolve electron density and temperature, and electrostatic potential at the outboard mid-plane via turbulent cross-field and classical parallel transport. In contrast to the core gyrokinetic models described above, it allows for strongly non-linear fluctuations (e.g. $\delta n/n \sim O(1)$) and corresponding phenomena such as 'blobs' and bursty cross-field transport. SOLT modelling of low-power NSTX ELM-free H-modes is able to recover the scaling of the parallel electron heat-flux width λ_q with input power, but does not capture the observed stronger scaling of λ_q with plasma current I_p [30, 96]. Using a synthetic gas puff imaging diagnostic to compare simulated fluctuation characteristics against measurements, it was concluded that mid-plane turbulence is the main contributor to the λ_q width in the low-power scenario, but that other phenomena such as MHD, X-point motion or divertor leg instabilities not included in SOLT are important players in setting the I_p scaling. Another example of non-linear edge turbulence model benchmarking includes comparisons of the ESEL code [97] (also a 2D fluid code) against probe measurements from the TCV tokamak, which found relatively good agreement in a number of quantities such as the predicted and measured distribution functions of density fluctuations and turbulent particle flux.

Looking to the future, the clear next step is to self-consistently integrate these individual physical processes and plasma regions into a single integrated predictive model. This integration is the goal of the proposed Fusion Simulation Program (FSP) [98], and initial steps towards this goal have been started by the protoFSP SciDAC programs. Of particular relevance to the turbulent transport processes described here are the Framework Application for Core-Edge Transport Simulations (FACETS) [58] and Center for Plasma Edge Simulation (CPES) [99, 100] projects, which have explored different formulations and frameworks for self-consistently integrating core and edge transport to both external sources and the thermal neutral population generated via wall recycling. To date both projects have only performed proof-of-principle simulations, and detailed validation studies remain to be undertaken. Nonetheless, they represent exciting advances towards translating physical understanding into a predictive capability.

Table 3 summarizes the core transport physics codes that are mentioned in this section, together with a brief description and references to more detailed explanations.

6. Innovative concepts

6.1. Snowflake divertors for power plants

The snowflake divertor is based on the use of PF configurations where the magnetic field null is second order, this meaning that not only the magnetic field components but also their first spatial derivatives become zero at the null-point. The shape of the separatrix near the null acquires then a characteristic hexagonal structure, reminiscent of a snowflake, whence the name. An analysis of this new geometry [101, 102] has shown that one can expect significantly larger PF flux expansion compared with the standard X-point divertor, and a significant increase in the connection length between the mid-plane and the divertor plates. This should lead to a corresponding increase in the radiative losses from the scrape-off region and significant reduction of the divertor heat fluxes [103]. These benefits are present even if the PF configuration does not correspond to an 'exact' snowflake, but is simply close enough to it [102], making the control of the PF configuration manageable [104].

The first experimental demonstration of the reduction of heat fluxes on divertor plates and much easier transition to detached regimes was achieved on the NSTX facility by Soukhanovskii *et al* [105]. Reduction of the heat fluxes was accompanied by an approximately two-fold decrease in the amount of impurities in the bulk plasma.

The proximity to the second-order null also gives rise to a significant increase in the magnetic shear just inside the separatrix, in the pedestal region [102, 106]. The increased shear, in turn, affects the stability of the pedestal region and provides a new technique to control the MHD activity at the plasma edge. How strong this effect can be was experimentally demonstrated on the TCV facility by Piras *et al* [107], where the transition from the standard X-point configuration to a near snowflake has led to reduction of the type-1 ELM frequency by a factor of 2–3, with the increase in the amplitude of the ELMs by only about 30%. This was achieved in the H-mode, and was accompanied by some additional improvement of the plasma confinement (compared with the H-mode with the standard X-point divertor). Importantly, experiments on TCV and NSTX were performed with the existing set of PF coils.

Heat-flux reduction in the snowflake configuration is attained not only via the larger PF flux expansion, but also by splitting of the flux between several strike points. In principle, by the use of a snowflake configuration, the outboard heat flux can be split between three strike points [108]. The reality of heat-flux splitting was demonstrated in experiments [105, 107].

In scaling the snowflake configuration to reactors, a critical issue is whether the snowflake can be created by a set of PF coils situated outside the shield and, desirably, outside the TF coils. First analyses [101, 102] have shown that this is indeed possible for ITER-scale facilities. It may become even easier for more compact devices. An overall design of a fusion reactor with the snowflake divertor is still an issue for future work. The most important aspects of this work would be design of a PF system allowing for flux splitting and significant reduction of the ELM-related component of the flux.

6.2. Liquid metal PFC development for power plants

Introduction. The material most often cited as a candidate for PFCs in a fusion reactor is tungsten. Even tungsten, however, requires significant materials development, in order to ensure that the PFCs have adequate lifetime under the combined flux of neutrons and plasma at the reactor wall. There are structural materials, such as reduced activation ferritic/martensitic (RAFM) steels, which show promise in high neutron dose environments [109], but for reactor PFCs steels are not generally considered attractive. A long cycle of development and testing of nanocomposited or other variants of tungsten would be required to qualify any material for reactor PFC applications.

If reactor PFCs could be renewed *in situ*, many restrictions on the choice of materials—for example, the allowable erosion rate—may be relaxed. One approach to a renewable PFC is to incorporate a layer of liquid metal as the plasma-facing surface. This was the focus of the ALPS (Advanced Liquid Plasma-facing Surface) and APEX (Advanced Power EXtraction) programs in the United States [110]. The leading candidates for liquid PFCs were metals with melting points near or below 200 °C, and low vapour pressure over a wide temperature range.

The use of a renewable liquid metal surface allows for a thinner interface between the PFC surface and the coolant. The PFC must still not be eroded faster than the fluid replacement time, but this replacement time will be minutes or seconds rather than years. Therefore, the use of even slowly flowing liquid metals will allow thin-walled divertor target constructions that can be cooled from behind. Other approaches, such as fast-flowing liquid metal jets or films, may also tolerate high-heat loading. In jet or fast-flowing design concepts, heat is removed with the flowing liquid metal (the system is 'self-cooled'), without a separate coolant loop. The use of evaporative cooling is another possible approach for lithium PFCs. Lithium forms a vapour shield at sufficiently high-heat flux. Self-shielding has been shown to permit operation of liquid lithium PFCs at very highly localized heat loads, even under long-pulse conditions [111]. Any such construction, whether a thin slowly flowing system or a thick fast-flowing jet or film, must also be able to withstand disruptive forces, although the liquid metal PFC itself could be reformed after a disruption.

Finally, the use of liquid metals may allow a shortened test cycle for reactor PFCs. Liquid metals are not subject to neutron damage, although the substrate supporting the flow is. Conversely, the substrate is not subject to PMI, although it must have sufficient lifetime in a fusion neutron environment. The use of liquid metal PFCs separates PMI from neutron damage issues, so that the liquid metal can be adequately tested in a non-nuclear tokamak, while the supporting structural system could, in principle, be tested in a fusion materials irradiation facility, which lacks the PMI component. For PMI testing, plasma exposure times that exceed the time it takes the liquid metal to flow from inlet to outlet (the residence time of the fluid in the tokamak) are unnecessary. This also reduces the required pulse length for PMI testing to of order 10–1000 s, and completely eliminates the need for high duty factor testing (at least for the liquid metal PFC).

However, no tokamak has yet demonstrated operation with full liquid metal PFCs. Important problems for the implementation of liquid metal PFCs are the difficulties of introducing the liquid metal to a tokamak, producing stable flow across the confining magnetic fields, and finally removing the liquid metal from the tokamak for purification, cooling or other processing. Because of the difficulties associated with generating such a flow in a fusion system, and the fact that the tokamaks which are currently testing liquid metal PFCs have pulse lengths on the order of a second or less, near-term experiments have focused on static liquid metal systems. Static liquid metal systems require renewal of the PFC between discharges only.

Liquid metals for PFCs. The most promising liquid metals for PFC applications are lithium, gallium and tin. Lithium and tin also form a eutectic, in the range 80% tin–20% lithium, which has possible advantages over either pure metal. At this time, however, most of the tokamak experiments in the world, which have employed liquid metals as PFCs, have concentrated on lithium, although a few experiments have been performed with gallium. Neither tin nor a tin–lithium eutectic has been investigated in a tokamak.

The physical properties of lithium, gallium and tin differ significantly, although all three metals have low melting points. Table 4 summarizes relevant properties of all three metals.

Lithium, gallium and tin span a wide range in atomic number, from the lowest Z of any solid (for lithium) to an

Table 4. Properties of candidate liquid metals.

	Lithium	Gallium	Tin
Atomic number	3	31	50
Atomic weight	6.9	69.7	118.7
Melting point (°C)	180.5	29.8	232.0
Boiling point (°C)	1342	2204	2602
Liquid density (g cm^{-3})	0.5	6.1	7.0
Specific heat capacity (J g^{-1} °C^{-1})	3.58	0.37	0.23
Thermal conductivity (W m^{-1} °C^{-1})	40.6	84.8	66.8
Electrical resistivity (140 nΩ m)	93	140	115
Temperature at which vapour pressure = 10^{-7} Torr (°C)	400	900	1000
Heat of vaporization (J g^{-1})	21 196	3673	2446

atomic number in excess of molybdenum (for tin). The specific heat capacity spans more than an order of magnitude, from tin (0.23 J g^{-1} °C^{-1}) to lithium, which at 3.58 J g^{-1} °C^{-1} has the highest specific heat of any material that is solid at room temperature. The limit in practical operating temperature for each of the metals is determined in part by the vapour pressure. An approximate limit is set by the temperature at which the equilibrium vapour pressure of the liquid equals 10^{-7} Torr; this limit is low for lithium (400 °C), but exceeds the maximum expected operating temperature for PFCs in a reactor for either gallium (900 °C), or tin (1000 °C).

Lithium would not be a serious candidate for a liquid metal PFC, due to its low operating temperature limit, if it did not offer the possibility of very low recycling. The performance advantages associated with low recycling lithium wall coatings have been noted since experiments in the Tokamak Fusion Test Reactor (TFTR) were conducted 20 years ago [112]. It is worth noting that current reactor design studies (e.g. the ARIES system designs) assume performance relevant to confinement scalings, which are associated with high recycling walls. These studies also assume a sufficiently high operating temperature for the PFCs and coolants to produce thermodynamic efficiencies of 50% or higher for power generation. The ARIES designs are therefore much more compatible with the use of high recycling liquid metals, such as gallium or tin. Design of reactors with liquid lithium walls, on the other hand, has focused on much smaller systems [113], which require enhanced confinement associated with low recycling walls in order to produce useful amounts of fusion power for use in fusion–fission hybrids, or small unit size fusion reactors. For a fusion reactor that employs lithium PFCs, it may be desirable to operate the blanket structure at a higher temperature than the PFCs in order to maintain good thermodynamic efficiency for power generation.

Not all structural materials are compatible with liquid metals. For example, gallium alloys with many metals, but does not readily attack ceramics. Tin is compatible with alumina and quartz, even at elevated temperatures, and with all the refractory and many common metals. Lithium is compatible with all the refractories, as well as vanadium, niobium and steels over the applicable temperature range (less than 450 °C), provided that impurities such as nitrogen are eliminated as the lithium is recirculated. But lithium attacks most ceramics above 400 °C, and will rapidly and destructively invade materials such as quartz or alumina. Known exceptions to this rule are yttria (Y_2O_3) and erbium oxide (Er_2O_3). Both of these ceramics have high binding energies, and are resistant to attack by liquid lithium up to temperatures of 600–700 °C.

Finally, although sodium is not suitable as a PFC, since it has unacceptably high vapour pressure when liquefied, it is of interest as a liquid metal coolant. Sodium is usable with many ceramics, and has been employed as a coolant in experimental fast fission reactors for decades.

Although solid lithium coatings have been used for wall conditioning in tokamak experiments since TFTR at the Princeton Plasma Physics Laboratory (PPPL) [112], and recently in the National Spherical Torus eXperiment (NSTX, also at PPPL) [114], it is only with a liquid PFC that the full lithium inventory is available for deuterium pumping. The diffusivity of deuterium in liquid lithium is high—of order 10^{-4} cm^2 s^{-1} over the temperature range of 300–400 °C [115], but is negligible in solid lithium. Experiments in T11-M at TRINITI, Troitsk, Moscow [116], the Current Drive eXperiment-Upgrade (CDX-U, at PPPL) [111] and the Frascati Tokamak Upgrade (FTU, at ENEA Frascati) [117] have all employed liquid lithium as a PFC, to varying degrees. Near-term experiments in the Lithium Tokamak eXperiment (LTX, at PPPL) [118] and NSTX [119] will make more extensive use of liquid lithium PFCs.

Summary. Liquid metal PFCs may offer an alternative to the use of tungsten in fusion reactors. Although the development of liquid metal systems for reactor use is in an early stage, the use of liquids may eliminate time-consuming qualification steps, which would likely be necessary for solid PFCs. It is, for example, clear that neutron damage to a continuously replaced liquid is not a concern. PMI with a substrate that supports the liquids is also not a concern, except for off-normal situations. The ultimate development cycle for liquid metal PFCs may therefore be shorter than the corresponding qualification cycle for solids.

Finally, this brief discussion of liquid metal PFCs is intended as a short introduction. More extensive treatments of liquid metal PFCs may be found in the proceedings of the 2009 International ITER Summer School [120] or in summaries of the US ALPS program [110, 121].

6.3. Carbon as a flow-through, consumable PFC material for fusion reactors

In progressing from present fusion devices to reactors, the annual energy load, $E_{\rm load}^{\rm year} \equiv P_{\rm heat}\tau_{\rm annual}$ will increase by ~five orders of magnitude (table 5), where $P_{\rm heat}$ (MW) is the heating power and $t_{\rm annual}$ (s yr^{-1}) is the annual run time. Thus the rate of gross erosion at the divertor strike points of a reactor could be roughly five orders of magnitude higher than in present devices. The measured rate of *net* erosion in present devices is 0.1–10 nm s^{-1} [122], thus for a typical 10^4 s yr^{-1} operation the rate of target surface recession is only ~10^{-6}–10^{-4} m yr^{-1}. However, if net erosion were also to scale up by five orders of magnitude then for reactors the rate of recession would be 0.1–10 m yr^{-1}, which is not acceptable. Fortunately, the plasma conditions foreseen at the divertor targets of devices such as ITER and FDF (Fusion Development Facility), $T_{\rm e} \sim 5$ eV and $n_{\rm e} \sim 10^{21}$ m^{-3}, are such as to

Table 5. Rough estimate of net erosion rate of main walls based on assumptions in the text; 100% wall coverage by Be, B, C or W is assumed. Other estimates: * from [123].

Device	P_{heat} (MW)	τ_{annual} run time (s yr^{-1})	E_{load}^{year} (TJ yr^{-1})	Beryllium net wall erosion rate (kg yr^{-1})	Boron net wall erosion rate (kg yr^{-1})	Carbon net wall erosion rate (kg yr^{-1})	Tungsten net wall erosion rate (kg yr^{-1})
DIII-D	20	10^4	0.2	0.13	0.11	0.08	0.16
JT-60SA	34	10^4	0.34	0.22	0.19	0.15	0.27
EAST	24	10^5	2.4	1.6	1.2	0.82	1.8
ITER	100	10^6	100	77 [29*]	64	44 [53*]	92 [41*]
FDF	100	10^7	1000	610	500	340	740
Reactor	400	2.5×10^7	10 000	6500	5300	3700	7900

strongly suppress net erosion relative to gross erosion due to prompt local deposition of sputtered particles: when the ionization mean free path for the sputtered impurity neutral L_{ioniz} is less than the fuel ion Larmor radius ρ_{DT}, then the strong E-field in the magnetic pre-sheath, of thickness $L_{MPS} = 33$–$10\rho_{DT}$, promptly returns the ionized impurity to the target. For $T_e \sim 5$ eV and $n_e \sim 10^{21}$ m^{-3}, $L_{ioniz} < L_{MPS}$ for both high-Z elements such as W and low-Z ones such as carbon.

Unfortunately the PFCs at the main vessel walls will not benefit from this effect since the plasma there is much less dense. Therefore, the net erosion $\sim$ gross erosion, the latter being due to charge exchange neutrals and (relatively) dilute plasma contact. Table 5 provides rough estimates for the wall erosion rate assuming: (i) physical sputtering by cx neutral tritons only; $E^{cx} = 300$ eV T_0 assumed, see [123]; (ii) normal incidence yields [124] doubled to account for surface roughness: for (Be, B, C, W), $Y^{cx} = (0.083, 0.056, 0.035, 0.0024)$; (iii) no sputtering included for D_0, He_0 or any plasma–wall contact (ionic); (iv) no chemical sputtering or radiation enhanced sublimation of C at reactor-relevant temperatures, of $\sim$700 °C $< T_{wall} <$ 1100 °C − 1900 °C [125]; (v) $P_{cx} = 0.05 P_{heat}$ [123], thus $0.025 P_{heat} = E^{cx}\varphi^{cx}$, where φ^{cx} is the particle flux to the walls. Thus, the gross erosion rate $= Y^{cx}\varphi^{cx} \approx$ the net erosion rate for the main wall.

In current tokamaks the main wall generally tends to be in a (spatially averaged) state of net erosion with the lost material being transported to the divertor where it accumulates [126]. In fact, in cold, detached conditions in DIII-D the entire divertor—both outer as well as inner targets—are in a state of net deposition due to PFC material migration from the walls [122]. It appears, therefore, that we may have been worrying about the wrong problem. There has been concern about the problem of net erosion at the strike points of reactors. It may be, however, that for reactor-relevant, high-power, high-density plasmas, the entire divertor will be in a state of net deposition due to migration of eroded wall material. Because of the large wall area, the wall erosion itself may be tolerable providing it is not highly localized. The problem, however, will be to clear the PFC slag out of the divertor rapidly enough to avoid disrupting plasma operation. In this case, it will be necessary that any acceptable PFC material be *flow-through*, like liquid Li. In particular, it will be as essential to be able to remove *in situ* the deposited PFC material as to introduce it in the first place.

Carbon, used as an *in situ* continuously replenished coating on a substrate which is resistant to neutron damage would appear to be potentially useable in this regard: (i) C is a solid refractory, yet (ii) it can be conveniently introduced and removed as cool gases: CH_4 (coating by chemical or physical vapour deposition or plasma-assisted CVD) and CO_2 (by O_2-baking [127] or O-plasma cleaning); (iii) carbon is satisfactory as a plasma-facing material; (iv) carbon is not satisfactory for prolonged exposure to neutrons, due to swelling damage, but the C would pass through the reactor before accumulating such a damage; (v) at reactor-relevant T_{wall} there is very little tritium retention in carbon, thus (v) very little DTO (a biological hazard) from O_2-baking; (vi) the quite possible incompatible requirement that a PFC material be satisfactory for both plasma and neutron interactions is dealt with by a 'division of labour': the substrate need not be plasma-compatible, opening up more options.

Estimates of net erosion rates and tritium codeposition rates have been made for a reactor: (i) net erosion is $\sim$3700 kgC yr^{-1}, see table 5; (ii) the D (T) thermal desorption peak for C is at $\sim$950 °C [128], thus there is very little T in C codeposits at $T_{wall} = 1000$ °C; (iii) for 1 atm O_2-baking at 700 °C, the removal rate is 2 gC m^{-2} s^{-1} [127]; (iv) if the C is deposited on 100 m^2, then the total annual C (and T) throughput would be recovered in a single 6 h O_2-bake, or faster using O-plasmas.

6.4. Self-passivating tungsten alloys for first wall applications

In a fusion power plant, the exposure of the first wall and structural materials to high neutron doses is a major additional challenge compared with current fusion experiments and even ITER. For ITER, at end-of-life the radiation damage due to neutrons is estimated to three displacements per atom (dpa), whereas for a fusion reactor 100–150 dpa are expected. As a consequence, transmutation reactions will occur to a significant degree. They will produce radioactive isotopes from the elements in the reactor materials during operation. In case of a loss-of-coolant accident (LOCA), the afterheat due to the nuclear decay reactions can lead to a temperature rise, approaching 1400 K at the first wall for a water or He-cooled reactor design after approximately 10–30 days [129]. Currently, tungsten materials are the best choice for PFCs at the first wall and in the divertor. At these temperatures, an additional air ingress into the reactor vessel leads to an oxidation of the tungsten materials, forming WO_3, which is highly volatile at these temperatures. Similar oxidation reactions occur for the W transmutation products Re and Os, which also form volatile oxides. As a consequence, radioactive isotopes are mobilized and pose a high radiation safety risk.

A solution is the use of self-passivating tungsten alloys, either as bulk materials or as a thick coating on steel wall components. During normal operation, the surface zone of these alloys is depleted in alloying elements by preferential sputtering. The sputtering yield for tungsten at low (several 10 eV) hydrogen isotope kinetic energies impinging at the surface is negligible, whereas alloying elements such as Si, Cr, Zr and Y are sputtered. The first wall surface therefore is enriched in tungsten, showing the desired respective low sputtering yields. Under off-normal conditions, as described above, the elevated temperatures accelerate diffusion of the alloying components, and oxidation reactions with air at the surface of the first wall materials occur. The alloying elements need to be selected such that the formed oxides are non-volatile and form a dense surface scale, which inhibits oxygen diffusion into the bulk or tungsten diffusion to the outer surface. Therefore, strongly reduced oxidation rates for tungsten are achieved and the bulk tungsten material is protected from continuous oxidation and evaporation of volatile WO_3 species.

The optimized composition of tungsten-based alloys with self-passivating properties is investigated by producing thin films of a few μm thickness in a magnetron sputtering device. Using up to four different magnetrons allows us to vary the composition of the deposited films in a flexible manner. The magnetron deposition technique provides alloys with a distribution of the constituents at atomic level without additionally required annealing steps. The model alloys are deposited either on inert alumina or quartz substrates. The oxidation behaviour is determined in a thermo-balance using dry synthetic air as oxidizing atmosphere slightly above ambient pressure with controlled gas flow. Temperature ramping up and down is performed in argon inert gas. The oxidation rates are calculated from the evaluation of the weight gain during the oxidation at a selected constant temperature. The composition of the model alloys is determined by Rutherford backscattering spectrometry with films with reduced thicknesses (300 nm), deposited under identical conditions on graphite substrates. Already the alloying of W by one element (Si) reduces the oxidation rate significantly. The reduction depends on the Si concentration and on the oxidation temperature. For 18 wt% Si concentration (WSi18), two orders of magnitude lower oxidation rates are measured compared with a pure W film of the same thickness [130]. Even higher reductions in oxidation rates can be achieved if a third alloy component is added. Zr, Y and Cr are compared and lowest oxidation rates are found for ternary W–Si–Cr alloys [131]. Here, the passivation mechanism is based on a dense layer of Cr_2O_3 formed at the surface during oxidation, together with a depletion of the layers below in Cr. In the ternary alloys, WO_3 is still detected in deeper layers, which can evaporate under LOCA conditions with high wall temperatures. The formation of WO_3 can be completely avoided and the oxidation rates even further reduced if a fourth alloying element is added. X-ray diffraction analysis for a W–Si3–Cr10–Zr5 quaternary alloy also forms a passivating Cr_2O_3 top surface layer, depleting the deeper layers in Cr. These layers, however, contain only WO_2, $CrWO_4$ and W, whereas no WO_3 (which has the highest vapour pressure and therefore evaporates most easily) can be detected. Figure 5 compares the linear oxidation rate of pure W with the several binary, ternary and quaternary alloys.

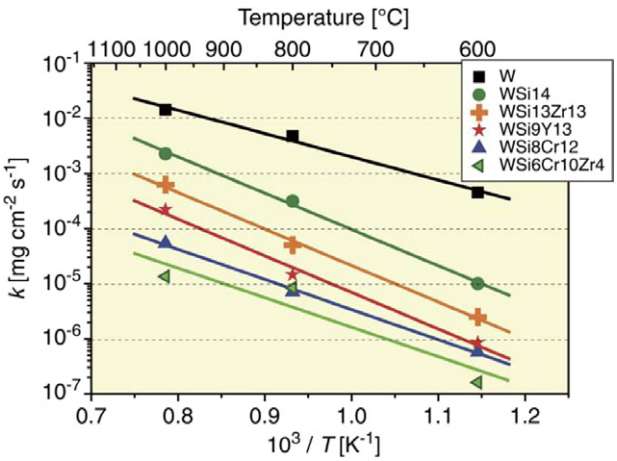

Figure 5. Arrhenius plot of the linear oxidation rates for pure W and selected binary, ternary and quaternary W-based alloys. Depending on the oxidation temperature, alloying reduces the oxidation rates by 3–4 orders of magnitude.

The successful development of self-passivating W-based alloys, based on composition variation, oxidation tests and further characterization on thin films on inert substrates needs to be transferred to bulk materials (thicknesses mm or larger). Since the reservoir of alloying elements is much larger than for thin films, it is expected that the concentration of alloying elements can be drastically reduced. Moreover, bulk materials allow us to characterize the thermo-mechanical behaviour of these alloys, including, e.g., thermal conductivity and elastic properties. The first attempts to produce ternary W–Si–Cr alloys by powder metallurgy were successful, but further investigations are necessary. Finally, it is required to study the properties of W-based alloys as first wall materials, in particular hydrogen retention and release and the interaction with other potential first wall materials.

7. New device contributions to edge physics understanding and benchmarking

A panel discussion was held to discuss the potential contributions from proposed new devices to resolving the plasma edge and materials interface issues for a reactor scenario. The panel consisted of representatives from three proposed devices and a representative from ITER. Talks were solicited from the three proponents of new devices summarizing the specific features of each. Two proposals are versions of a FNSF, one at low aspect ratio and one at moderate conventional aspect ratio. These are intended to address a wide variety of fusion science issues, including the tritium cycle, maintenance and plasma control, as well as the materials issues. The third proposal is for a more dedicated plasma materials interface (PMI) facility, NHTX, intended to operate as a non-nuclear facility, but with hot walls. Whereas ITER will look at very long-pulse issues at high energy gain, all three are essentially long-pulse experiments designed to look at true steady state with varying energy gain, and should be capable of confronting the long-term issues of the interaction of the plasma and the external material surfaces. A fourth proposal, VULCAN, was also mentioned in the discussions

but was not described in a formal presentation. Nevertheless, it is relevant to the discussion and is included here.

Both the low aspect ratio and moderate aspect ratio FNSF are designed to provide an environment that can be used to support materials testing in a fusion environment. The goal is to investigate the synergistic effects of plasma–surface interactions and provide solutions to issues of high alpha particle, neutron, and hydrogenic ion fluxes and heat fluxes, sputtering, erosion, hydrogenic redeposition and migration issues, and He implantation. The proposed devices will also study the effects of large thermal gradients and thermal stresses on materials, bulk radiation damage, including tritium trapping, radiation-induced changes and transmutations, and the consequent degradations in thermo-mechanical properties. It will also address engineering issues of the effects of multiple materials, joints, and interfaces, corrosion and contamination. High wall temperature, $T \sim 700\,^{\circ}\mathrm{C}$, is crucial for studying the issues of long-term hydrogen isotope retention; there is currently little or no focus on this issue in the existing international fusion programme. Although the upcoming steady-state facilities EAST and KSTAR will address some steady-state PMI issues, the heating power levels, first wall temperature, pulse length and duty factor fall short of what is needed to support the design of a component test facility or pilot plant, let alone DEMO.

The moderate aspect ratio FNSF option FDF [132] is envisioned as an aspect ratio 3.5 tokamak with major radius $R_0 = 2.7\,\mathrm{m}$, directly following on from DIII-D and Alcator C-Mod with the construction features of those two machines, and is about 50% larger than DIII-D and about 40% the size of ITER. The coil design is topologically equivalent to DIII-D. The outermost element is a massive copper toroidal coil, steady-state water cooled and capable of 6 T. The TF coil is constructed of plates like DIII-D and Alcator C-Mod, which enables easy steady-state water or oil cooling. A demountable coil will allow the top to be taken off the machine remotely for full maintenance accessibility.

The FDF is intended to run in an advanced tokamak mode, with normalized beta $\beta_N \sim 3.7$. The auxiliary power is capable of up to 54 MW. With a baseline total plasma current of 6.6 MA, the bootstrap fraction is 75%, requiring 42 MW to drive the remaining 25% of the current. In advanced mode, the current is increased to 7.4 MA and the bootstrap fraction is 90% with only 32 MW auxiliary power. The density is 60% of the Greenwald limit in baseline mode and 86% in advanced mode, which enables reasonable current drive efficiency. The confinement factor H_{98y2} is 1.6, comparable to what DIII-D achieves on very long-pulse plasmas. The envisaged advanced tokamak operating modes will require a complete control system and can be used to study off-normal events under burning plasma conditions. The design includes non-axisymmetric coils for ELM and resistive wall mode control and options for advanced divertors. The total power to run the entire facility is about 500 MW in either mode. First wall materials and structures and near first wall components such as RF launchers and diagnostics can be developed in a fusion-relevant environment. FDF is also expected to be compatible with ELM-free QH-mode operation.

The energy gain ranges from $Q \sim 6.9$ in baseline mode to $Q \sim 20$ in the most aggressive advanced mode. With operating durations of up to 2 weeks for a duty factor of 30%, FDF will demonstrate the whole fuel cycle including extraction, accountability, and safety issues of a steady-state DT device to pave the way for DEMO. A key additional feature of FDF is that a primary goal is the generation of a significant tritium inventory that will be needed for initial DEMO reactor operation. FDF will be designed for a neutron flux at the outer mid-plane of 1–2 $\mathrm{MW\,m^{-2}}$ and will have a goal of an integrated fluence of 3–6 $\mathrm{MW\,yr\,m^{-2}}$ over 10 years of operation. This results in about 10 times the time-integrated peak neutron fluence of ITER, or about 1/50 of the fluence expected during the life of a power plant (table 1).

FDF will be designed with the flexibility and maintainability to allow ten test blanket variations to be tested over the facility lifetime and one or two change-outs of the main full tritium producing blanket. Test cells for material sample volumes for a total of about $10\,\mathrm{m^3}$. FDF can enable irradiation qualification of materials in port material sample exposure stations. Hot walls with $T \sim 700\,^{\circ}\mathrm{C}$ will allow studies of tritium retention under reactor conditions.

The low aspect ratio version [133] envisages a 1.3 m major radius with $A \sim 1.7$. This would also necessarily have many advanced tokamak features, with a bootstrap fraction of around 0.5 and with operation at successively higher plasma pressures ranging initially from a JET-like normalized beta of $\beta_N \sim 2$ ($\beta = 4.4\%$) up to $\beta_N \sim 3.5$ ($\beta = 11\%$) in full operation as the TF is ramped from 2.7 up to 3.6 T and the plasma current from 4.2 MA in the initial phase, to 8.4 MA for a total fusion power output of 150 MW and wall loadings of $2\,\mathrm{MW\,m^{-2}}$.

The key argument for a dedicated non-nuclear PMI facility such as NHTX [134] is that it would address the three most important PMI issues simultaneously: high-power density, long pulse and hot walls. A non-nuclear facility with hot walls will provide increased configurational flexibility than a device that also includes a nuclear mission. The NHTX is proposed with an aspect ratio $A \sim 2$, major radius = 1 m, TF $B = 2\,\mathrm{T}$, plasma current $I = 3$–$4\,\mathrm{MA}$, heating power of 40–50 MW, surface-averaged power flux P/S up to $1\,\mathrm{MW\,m^{-2}}$, a pulse length of 10^3–10^6 s and wall temperature up to $T \sim 700\,^{\circ}\mathrm{C}$. It would be built with steady-state water-cooled Cu coils and have large outboard mid-plane ports for diagnostic access and maintenance of internal components. The upper TF coils would be demountable and vessel top lid removable for large-scale modification or replacement of the PFCs and divertor structures. The ex-vessel poloidal field coil set has been designed to be compatible with a range of divertor configurations ranging from ITER-like lower single-null, balanced double-null, a 'snow-flake' divertor and X/Super-X divertor configurations. In addition, both hot high-Z walls and liquid metal PFCs can also be tested with the internal space provided in the design. For a liquid metal PFC programme in NHTX, it is proposed that both capillary porous and fast-flowing liquid metal divertor targets should be tested, including assessment of liquid-surface stability and surface temperature limits, as well as development of techniques to ensure that metal does not accumulate in the vacuum vessel. The motivation for limiting NHTX operation to primarily H/D is to enable hands-on in-vessel access for H operation and ex-vessel hands-on access for D operation. This choice should accelerate the PMI research programme by reducing the

need for nuclear shielding, remote maintenance and hot cells, thereby reducing the size and cost of the base device compared with fusion-capable FNSF devices. While operating primarily in H and D, trace-tritium capabilities for precise measurement and verification of hydrogenic retention and diffusion are also envisioned near the end of a successful PMI/PFC development programme.

Another device proposed for PMI research is VULCAN [135] which also incorporates long-pulse, high-heat-flux, hot-wall capabilities, but with higher aspect ratio $A = 4$ and with high-temperature superconducting (HTS) coils. The proposed device parameters are $R = 1\,\mathrm{m}$, $B_\mathrm{T} = 7\,\mathrm{T}$, $I_\mathrm{p} = 1.5\,\mathrm{MA}$, $P_\mathrm{aux} = 14\,\mathrm{MW}$ and $P/S = 1\,\mathrm{MW\,m^{-2}}$. Because of the use of superconducting coils, the device could in principle run in steady state with reduced electricity consumption. Demountable HTS coils are also being investigated as a means of providing improved maintenance and machine flexibility. Like NHTX, the device mission would be to investigate issues such as fuelling balance and retention, recycling characteristics with fully depleted hot walls, safety issues with flakes and dust, impurity control in the limit of negligible vacuum impurities (water, carbon dioxide, etc), the role of high-Z materials on fuel permeation and sputtering, and erosion control for conditions in which the wall materials have been fundamentally modified by continuous plasma operation.

All four facilities would enable specifically plasma edge–material surface interactions to be explored under long-pulse conditions, enable exploration of options, and materials testing, and provide essential data for benchmarking simulations of reactor conditions. The general consensus was that either a FNSF or a dedicated PMI facility would reduce the risk of the large step between ITER and a DEMO, but likely with increased total planned cost, although the actual costs without such a facility may, of course, be higher if the risks are realized. The dedicated PMI facility was claimed to provide the lowest risk in terms of the plasma–materials interface issues with the lowest cost but the FNSF options would also address a number of additional critical issues.

8. Summary

The plasma–material interface has been an important consideration in the operation of experimental confinement devices since the earliest days of the fusion programme. If anything, the challenge has become even larger in the ITER era. It will not be possible to build many large experimental facilities to test and demonstrate edge physics in the power plant regime, which is expected to be even more demanding on materials and on plasma control. A strong physics basis together with improved modelling and benchmarking on available devices will be needed to reduce the risk in extrapolating to DEMO.

This workshop described progress and remaining challenges in the related areas of plasma edge physics and plasma–material interactions, for technical topics involving edge physics, plasma modelling, experimental benchmarking, innovative concepts and possible contributions of proposed new devices. The existing models and experimental database are not yet adequate to predict edge power flows and material behaviour in the power plant regime of tokamak operation with any confidence. Further fundamental research is needed, as is a strengthened activity to keep research focused on the issues and parameters of most importance to fusion energy production.

Acknowledgments

The authors would like to thank all of the participants in the Town Meeting, with special thanks to colleagues C.P. Wong, T.E. Evans and A. Leonard for providing comments and significant input to table 1. This work was supported in part by the US Department of Energy under Cooperative Agreement No DE-FC02-04ER54698, DE-AC02-09CH11466, and grant number DE-FG02-04ER54757.

References

[1] Raffray A.R. *et al* 2010 *Fusion Eng. Des.* **85** 93–108
[2] ITER Physics Basis Editors *et al* 1999 *Nucl. Fusion* **39** 2137
[3] Shimada M. *et al* 2007 Progress in the ITER Physics Basis: chapter 1. Overview and summary *Nucl. Fusion* **47** S1
[4] Kessel C.E. *et al* 2009 *Nucl. Fusion* **49** 085034
[5] Kessel C.E. *et al* 2009 *Nucl. Fusion* **49** 085034
[6] Pitts R.A. *et al* 2011 *J. Nucl. Mater.* **415** S957–64
[7] Leonard A.W. *et al* 2006 *Plasma Phys. Control. Fusion* **48** A149–62
[8] Baylor L.R. *et al* 2007 *Nucl. Fusion* **47** 443–8
[9] Evans T.E., Moyer R.A. and Monat P 2002 *Phys. Plasmas* **9** 4957–67
[10] Oyama N. *et al* 2006 *Plasma Phys. Control. Fusion* **48** A171–81
[11] Rapp J. *et al* 2009 *Nucl. Fusion* **49** 095012
[12] Burrell K.H. *et al* 2009 *Nucl. Fusion* **49** 085024
[13] Suttrop W. *et al* 2003 *Plasma Phys. Control. Fusion* **45** 1399–416
[14] Whyte D.G. *et al* 2010 *Nucl. Fusion* **50** 105005
[15] Greenwald M. *et al* 1999 *Phys. Plasmas* **6** 1943
[16] Matthews G. 1995 *J. Nucl. Mater.* **220–222** 104–16
[17] Stangeby P.C. 1993 *Nucl. Fusion* **33** 1695
[18] Kukushkin A. *et al* 2003 *Fusion Eng. Des.* **65** 355
[19] Jakubowski M.W. *et al* 2009 *Nucl. Fusion* **49** 095013
[20] Kessel C.E. *et al* 2013 The evaluation of the heat loading from steady, transient and off-normal conditions in ARIES power plants *Fusion Sci. Technol.* at press
[21] Nygren R. *et al* 2011 *J. Nucl. Mater.* **417** 451–6
[22] Tillack M.S., Raffray A.R., Wang X.R., Malang S., Abdel-Khalik S., Yoda M. and Youchison D. 2011 *Fusion Eng. Des.* **86** 71–98
[23] Hazeltine R.D. 2010 *Fusion Eng. Des.* **85** 1016–26
[24] LaBombard B. *et al* 2011 *J. Nucl. Mater.* **415** S349–52
[25] Brunner D. *et al* 2011 *J. Nucl. Mater.* **415** S375–8
[26] Lasnier C.J. *et al* 2011 *J. Nucl. Mater.* **415** S353–6
[27] Makowski M. *et al* 2011 *J. Nucl. Mater.* **415** S357–9
[28] Gray T.K. *et al* 2011 *J. Nucl. Mater.* **415** S360–4
[29] Mossessian D.A. *et al* 2003 *Phys. Plasmas* **10** 689
[30] Myra J.R. *et al* 2011 *J. Nucl. Mater.* **415** S605–8
[31] Goldston R.J. *et al* 2011 *J. Nucl. Mater.* **415** S566–9
[32] Burrell K.H. *et al* 2005 *Phys. Plasmas* **12** 056121
[33] Burrell K.H. *et al* 2009 *Phys. Rev. Lett.* **102** 155003
[34] Garofalo A.M. *et al* 2011 *Nucl. Fusion* **51** 083018
[35] Fenstermacher M. *et al* 2008 *Phys. Plasmas* **15** 056122
[36] Oyama N. *et al* 2005 *Nucl. Fusion* **45** 871
[37] McDermott R.M. *et al* 2009 *Phys. Plasmas* **16** 056103
[38] Porte L. *et al* 2007 *Nucl. Fusion* **47** 952
[39] Maingi R. *et al* 2009 *Phys. Rev. Lett.* **103** 075001
[40] Tobita K. *et al* 2009 *Nucl Fusion* **49** 075029
[41] Kawashima H., Shimizu K., Takizuka T., Tobita K., Nishio S., Sakurai S. and Takenaga H. 2009 *Nucl Fusion* **49** 065007
[42] Post D., Abdallah J., Clark R.E.H. and Putvinskaya N. 1995 *Phys. Plasmas* **2** 2328

[43] Asakura N. *et al* 2010 *J. Plasma Fusion Res. Ser.* **9** 136–41 www.jspf.or.jp/JPFRS/PDF/Vol9/jpfrs2010_09-136.pdf
[44] Rognlien T.D. and Rensink M.E. 2002 *Fusion Eng. Design* **60** 497
[45] Rognlien T.D., Rensink M.E. and Smith G.R. 2000 User Manual for the UEDGE edge-plasma transport code *Lawrence Livermore National Lab Report* UCRL-ID-137121 http://e-reports-ext.llnl.gov/pdf/246621.pdf
[46] Lao L.L., Ferron J.R., Geoebner R.J., Howl W, St John H.E., Strait E.J. and Taylor T.S. 1990 *Nucl. Fusion* **30** 1035
[47] Rognlien T.D., Bulmer R.H., Rensink M.E. and Brooks J.N. 2007 *J. Nucl. Mater.* **363–365** 658
[48] Braginskii S.I. 1965 Transport processes in a plasma *Reviews of Plasma Physics* vol 1 ed M.A. Leontovich (New York: Consultants Bureau) p 205
[49] Rognlien T.D., Ryutov D.D., Mattor N. and Porter G.D. 1999 *Phys. Plasmas* **6** 1851
[50] Scott H.A. and Adams M.L. 2004 *Contrib. Plasma Phys.* **44** 51–6
[51] Porter G.D., Rognlien T.D., Rensink M.E., Wolf N.S. and Stangeby P.C. 2005 *Fusion Sci. Technol.* **48** 1127 http://epubs.ans.org/?a=1065
[52] Smirnov R.D. *et al* 2010 *Contrib. Plasma Phys.* **50** 299
[53] Pigarov A.Yu., Krasheninnikov S.I., LaBombard B. and Rognlien T.D. 2007 *J. Nucl. Mater.* **363–365** 643
[54] Takenaga H. *et al* 2005 *Nucl. Fusion* **45** 1618
[55] Rognlien T.D., Umansky M.V., Xu X.Q., Cohen R.H. and LoDestro L.L. 2005 *J. Nucl. Mater.* **337–339** 327
[56] Brooks J.N., Allain J.P. and Rognlien T.D. 2006 *Phys. Plasmas* **13** 122502
[57] Pigarov A.Yu. and Krasheninnikov S.I. 2009 *J. Nucl. Mater.* **390–391** 192–5
[58] Cary J.R. *et al* 2009 *J. Phys.: Conf. Ser.* **180** 012056
[59] Batishchev O.V. *et al* 1997 *Phys. Plasmas* **4** 1672
[60] Xu X.Q., Bodi K., Cohen R.H., Krasheninnikov S. and Rognlien T.D. 2010 *Nucl. Fusion* **50** 064003
[61] Chang C.S. and Ku S. 2004 *Phys. Plasmas* **11** 5626
[62] Dorr M.R. *et al* 2010 Numerical simulation of phase space advection in gyrokinetic models of fusion plasmas *Proc. 2010 SciDAC Conf. (Chattanooga, TN, 11–15 July 2010)* http://computing.ornl.gov/workshops/scidac2010/papers.shtml
[63] Stangeby P.C. 2000 *The Plasma Boundary of Magnetic Fusion Devices* (Philadelphia, PA: Institute of Physics Publishing)
[64] Heifetz D.B. 1986 *Physics of Plasma–Wall Interactions in Controlled Fusion* ed D.E. Post and R. Behrisch (New York: Plenum)
[65] Coster D.P., Bonnin X., Mutzke A., Schneider R. and Warrier M. 2007 *J. Nucl. Mater.* **363–365** 136
[66] Loch S.D., Ballance C.P., Pindzola M.S. and Stotler D.P. 2009 *Plasma Phys. Control. Fusion* **51** 105006
[67] Krstic P.S. and Schultz D.R. 1998 *Atomic and Plasma–Material Interaction Data for Fusion* vol 1 (*Suppl. J. Nucl. Fusion*) (Vienna: IAEA) p 1 www-pub.iaea.org/MTCD/Publications/PDF/Pub23_web.pdf
[68] Loch S.D. *et al* 2006 *At. Data Nucl. Data Tables* **92** 813
[69] Loch S.D. *et al* 2008 *At. Data Nucl. Data Tables* **94** 257
[70] Janev R.K. *et al* 1987 *Elementary Processes in Hydrogen–Helium Plasmas* (New York: Springer)
[71] Sawada K. and Fujimoto T. 1995 *J. Appl. Phys.* **78** 2913
[72] Kukushkin A.S., Pacher H.D., Kotov V., Reiter D., Coster D. and Pacher G.W. 2005 *Nucl. Fusion* **45** 608
[73] Reiter D. *et al* 2007 *J. Nucl. Mater.* **363–365** 649
[74] Janev R.K. and Reiter D. 2002 *Phys. Plasmas* **9** 4071
[75] Janev R.K. and Reiter D. 2004 *Phys. Plasmas* **11** 780
[76] Reiter D., Kuppers B. and Janev R.K. 2009 *Phys. Scr.* **T138** 014014
[77] Pitts R.A. *et al* 2009 *Phys. Scr.* **T138** 014001
[78] Wischmeier M. *et al* 2009 *J. Nucl. Mater.* **390–391** 250
[79] Post D.E. 1995 *J. Nucl. Mater.* **220–222** 143
[80] Adams M.L. and Scott H.A. 2004 *Contrib. Plasma Phys.* **44** 262
[81] Park G.Y. *et al* 2007 *J. Phys.: Conf. Ser.* **78** 012087
[82] Staebler G.M., Kinsey J.E. and Waltz R.E. 2007 *Phys. Plasmas* **14** 055909
[83] Kinsey J.E., Staebler G.M. and Waltz R.E. 2008 *Phys. Plasmas* **15** 055908
[84] The ITER 1D Modelling Working Group 2000 *Nucl. Fusion* **40** 1955
[85] Waltz R.E., Staebler G.M., Dorland W., Hammett G.W., Kotschenreuther M. and Konings J.A. 1997 *Phys. Plasmas* **4** 2482
[86] Candy J., Holland C., Waltz R.E., Fahey M.R. and Belli E. 2009 *Phys. Plasmas* **16** 060704
[87] Barnes M., Abel I.G., Dorland W., Görler T., Hammett G.W. and Jenko F. 2010 *Phys. Plasmas* **17** 056109
[88] Candy J. and Waltz R.E. 2003 *J. Comput. Phys.* **186** 545
[89] Dorland W., Jenko F., Kotschenreuther M. and Rogers B.N. 2000 *Phys. Rev. Lett.* **85** 5579
[90] Holland C., White A.E., McKee G.R., Shafer M.W., Candy J, Waltz R.E., Schmitz L. and Tynan G.R. 2009 *Phys. Plasmas* **16** 052301
[91] Snyder P.B., Wilson H.R., Ferron J.R., Leonard A.W., Osborne T.H., Turnbull A.D., Mossessian D., Murakami M. and Xu X.Q. 2002 *Phys. Plasmas* **9** 2037
[92] Snyder P.B. *et al* 2009 *Nucl. Fusion* **49** 085035
[93] Snyder P.B., Groebner R.J., Leonard A.W., Osborne T.H. and Wilson H.R. 2009 *Phys. Plasmas* **16** 056118
[94] Snyder P.B. and Hammett G.W. 2001 *Phys. Plasmas* **8** 744
[95] Russell D.A., Myra J.R. and D'Ippolito D.A. 2009 *Phys. Plasmas* **16** 122304
[96] Myra J.R. *et al* 2011 *Phys. Plasmas* **18** 012305
[97] Garcia O.E., Horacek J., Pitts R.A., Nielsen A.H., Fundamenski W., Graves J.P., Naulin V. and Rasmussen J.J. 2006 *Plasma Phys. Control. Fusion* **48** L1
[98] Post D.E., Batchelor D.B., Bramley R.B., Cary J.R., Cohen R.H., Colella P. and Jardin S.C. 2004 *J. Fusion Energy* **23** 1
[99] Cummings J. *et al* 2008 *Commun. Comput. Phys.* **4** 675 www.global-sci.com/freedownload/v4_675.pdf
[100] Chang C.S. *et al* 2009 *J. Phys.: Conf. Ser.* **180** 012057
[101] Ryutov D.D. 2007 *Phys. Plasmas* **14** 064502
[102] Ryutov D.D. *et al* 2008 *Phys. Plasmas* **15** 092501
[103] Umansky M.V. *et al* 2009 *Nucl. Fusion* **49** 075005
[104] Kolemen E. *et al* 2010 *Nucl. Fusion* **50** 105010
[105] Soukhanovskii V.A. *et al* 2011 *Nucl. Fusion* **51** 012001
[106] Piras F. *et al* 2009 *Plasma Phys. Control. Fusion* **51** 055009
[107] Piras F. *et al* 2010 *Phys. Rev. Lett.* **105** 155003
[108] Ryutov D.D., Makowski M.A. and Umansky M.V. 2010 *Plasma Phys. Control. Fusion* **52** 105001
[109] Gelles D.S. 1996 *J. Nucl. Mater.* **233–237** 293–8
[110] Abdou M, Morley N and Sawan M 2004 *Fusion Eng. Des.* **72** 1–326
[111] Khripunov B.I. *et al* 2003 *Fusion Eng. Des.* **65** 449–54
[112] Mansfield D.K. *et al* 2001 *Nucl. Fusion* **41** 1823–34
[113] Zakharov L.E., Gorelenkov N.N., White R.B., Krasheninnikov S.I. and Pereverzev G.V. 2004 *Fusion Eng. Des.* **72** 149–68
[114] Kugel H.W. *et al* 2008 *Phys. Plasmas* **15** 056118
[115] Moriyama H, Iwasaki K and Ito Y 1992 *J. Nucl. Mater.* **191–194** 190–3
[116] Evtikhin V.A. *et al* 2002 *Plasma Phys. Control. Fusion* **44** 955–78
[117] Apicella M.L. *et al* 2007 *J. Nucl. Mater.* **363–365** 1346–51
[118] Majeski R. *et al* 2009 *Nucl. Fusion* **49** 055014
[119] Kugel H.W. *et al* 2009 *Fusion Eng. Des* **84** 1125–9
[120] Majeski R. 2009 Plasma interaction in controlled fusion devices *Proc. 3rd ITER Int. Summer School (Aix-en-Provence, France, 22–26 June 2009)*; 2010 *AIP Conf. Proc.* **1237** 122–37
[121] Brooks J.N. *et al* 2005 *Fusion Sci. Technol.* **47** 669–77
[122] Whyte D.G. 2005 *Fusion Sci. Technol.* **48** 1096

[123] Kukushkin A.S. 2008 *ITER Report* ITER_D_27TKC6, 14 April 2008
[124] Eckstein W. 2002 Calculated sputtering, reflection and range values *Report* IPP 9/32
[125] Stangeby P.C. 2000 *The Plasma Boundary of Magnetic Fusion Devices* (Bristol: Institute of Physics Publishing) chapter 3
[126] Kreter A. *et al* 2009 *J. Nucl. Mater.* **390–391** 38
[127] Davis J.W. and Haasz A.A. 2001 *Phys. Scr.* **T91** 33
[128] Davis J.W. and Haasz A.A. 1995 *J. Nucl. Mater.* **220–222** 832
[129] Maisonnier D. *et al* 2004 A conceptual study of commercial fusion power plants *Final Report* EFDA-RP-RE-5.0
[130] Koch F. and Bolt H. 2007 *Phys. Scr.* **T128** 100
[131] Koch F., Köppl S. and Bolt H. 2009 *J. Nucl. Mater.* **386–388** 572
[132] Chan V.S. *et al* 2010 *Proc. 23rd Int. Conf. on Fusion Energy 2010 (Daejeon, Korea, 2010)* (Vienna: IAEA) CD-ROM file FTP/2-3Rb and www-naweb.iaea.org/napc/physics/FEC/FEC2010/html/index.htm
[133] Peng Y.K.M. *et al* 2010 *Proc. 23rd Int. Conf. on Fusion Energy 2010 (Daejeon, Korea, 2010)* (Vienna: IAEA) CD-ROM file FTP/2-3Ra and www-naweb.iaea.org/napc/physics/FEC/FEC2010/html/index.htm
[134] Goldston R.J. *et al* 2008 *Proc. 22nd Int. Conf. on Fusion Energy 2008 (Geneva, Switzerland, 2008*) (Vienna: IAEA) CD-ROM file FT/P3-12 and www-naweb.iaea.org/napc/physics/FEC/FEC2008/html/index.htm
[135] Olynyk G.M. *et al* 2012 *Fusion Eng. Des.* **87** 224–33